NEUROPHYSIOLOGY

# Parabrachial neuron types categorically encode thermoregulation variables during heat defense

Wen Z. Yang[1,2*†], Xiaosa Du[1,3,4*], Wen Zhang[3*], Cuicui Gao[1,3,4*], Hengchang Xie[1,3,4], Yan Xiao[5,6], Xiaoning Jia[1‡], Jiashu Liu[1], Jianhui Xu[7], Xin Fu[1,3,4], Hongqing Tu[1,3,4], Xiaoyu Fu[1,3,4], Xinyan Ni[1], Miao He[8], Jiajun Yang[5,6], Hong Wang[9], Haitao Yang[1], Xiao-hong Xu[3], Wei L. Shen[1†]

Copyright © 2020 The Authors, some rights reserved; exclusive licensee American Association for the Advancement of Science. No claim to original U.S. Government Works. Distributed under a Creative Commons Attribution NonCommercial License 4.0 (CC BY-NC).

**Heat defense is crucial for survival and fitness. Transmission of thermosensory signals into hypothalamic thermoregulation centers represents a key layer of regulation in heat defense. Yet, how these signals are transmitted into the hypothalamus remains poorly understood. Here, we reveal that lateral parabrachial nucleus (LPB) glutamatergic prodynorphin and cholecystokinin neuron populations are progressively recruited to defend elevated body temperature. These two nonoverlapping neuron types form circuits with downstream preoptic hypothalamic neurons to inhibit the thermogenesis of brown adipose tissues (BATs) and activate tail vasodilation, respectively. Both circuits are activated by warmth and can limit fever development. The prodynorphin circuit is further required for regulating energy expenditure and body weight homeostasis. Thus, these findings establish that the genetic and functional specificity of heat defense neurons occurs as early as in the LPB and uncover categorical neuron types for encoding two heat defense variables, inhibition of BAT thermogenesis and activation of vasodilation.**

## INTRODUCTION

Homeostatic control of body temperature during heat defense is crucial for the survival and fitness of mammals. Heat defense–related disorders, including heatstroke and menopause thermal disequilibrium (MTD), are frequently seen in patients (*1*, *2*). Heatstroke causes hundreds of death each year in the United States (*1*, *3*), and MTD affects 75% of menopaused women (*2*, *4*). Because of the paucity of knowledge, there is only limited treatment for these disorders (*2*, *3*). Heat defense is achieved by precise coordination between dedicated central pathways and peripheral effector organs (*5*, *6*). Perturbation of these pathways may lead to temperature dysregulations (*7*) and aggravate obesity and type 2 diabetes (*8*). Previous findings have suggested that feed-forward temperature signals are detected by thermoreceptors expressed in dorsal root ganglion neurons (*9*) and are transmitted into the spinal cord (*10*), which then are relayed by lateral parabrachial nucleus (LPB) neurons in the brainstem (*11*–*13*) before reaching the preoptic area (POA) (*12*, *13*). Several key types of POA neurons have been identified recently to control different aspects of heat defense activity (*14*–*23*), including activation in vasodilation (*19*, *20*), reduction of physical activity and energy expenditure (EE) (*16*, *18*), reduction of brown adipose tissue (BAT) thermogenesis (*19*, *23*), and suppression of muscle shivering activity (*23*). Collectively, it demonstrates that the POA is the thermoregulatory center to control diverse thermoregulatory variables. However, the circuitry that provides key inputs to the POA to coordinately control these variables remains poorly understood.

The LPB is involved in regulating a series of physiological activities, including thermoregulation (*12*, *13*, *24*, *25*), pain and itch (*26*, *27*), food intake (*28*, *29*), blood glucose (*30*, *31*), and wakefulness (*32*). For example, cholecystokinin (CCK) neurons that coexpress leptin receptor (LepR) are sensitive to hypoglycemia and function to restore blood glucose levels via forming a circuit with SF1 neurons in the ventromedial hypothalamus (*30*, *31*). Pioneering work suggests that cutaneous warm and cold sensory signals are conveyed from the LPB to the POA by glutamatergic transmission via two distinct divisions, namely, the LPBd (dorsal) and the LPBel (external lateral) (*12*, *13*, *25*). While most cold-activated neurons in the LPBel are FoxP2$^+$, half of the warm-activated neurons in the LPBd are prodynorphin$^+$ (Pdyn$^+$) (*24*). Chemogenetic activation of these Pdyn neurons induces hypothermia (*33*). However, it is still unknown whether and how the LPB is involved in differential regulation of different heat defense variables.

To address the questions, we combined projection-specific transcriptome analysis with functional studies to define key elements of the LPB→POA circuitry during heat defense. We found that LPB Pdyn neurons and CCK neurons are progressively recruited in response to increasing temperatures. These two types of neurons categorically encode the inhibition of BAT thermogenesis and the activation of tail vasodilation, respectively. Both types can inhibit muscle shivering and limit fever development. In addition, Pdyn neurons are required for the body weight gain driven by a high-fat diet (HFD), suggesting a strong interconnection between homeostatic thermoregulation and weight control systems.

[1]Shanghai Institute for Advanced Immunochemical Studies and School of Life Science and Technology, Shanghaitech University, Shanghai 201210, China. [2]CAS Key Laboratory of Synthetic Chemistry of Natural Substances, Shanghai Institute of Organic Chemistry, Chinese Academy of Sciences, Shanghai 200032, China. [3]Institute of Neuroscience, State Key Laboratory of Neuroscience, CAS Center for Excellence in Brain Science and Intelligence Technology, Chinese Academy of Sciences, Shanghai, 200031, China. [4]University of Chinese Academy of Sciences, Beijing 100049, China. [5]Department of Neurology, Shanghai Jiao Tong University Affiliated Sixth People's Hospital, Shanghai 200233, China. [6]Department of Neurology, Shanghai Sixth People's Hospital East Affiliated to Shanghai University of Medicine and Health Science, 222 West Third Road, Huanhu, Shanghai 201306, China. [7]Thermoregulation and Inflammation Laboratory, Chengdu Medical College, Chengdu Sichuan 610500, China. [8]Institutes of Brain Science, State Key Laboratory of Medical Neurobiology, Fudan University, Shanghai 200032, China. [9]Shenzhen Key Laboratory of Drug Addiction, CAS Key Laboratory of Brain Connectome and Manipulation, the Brain Cognition and Brain Disease Institute (BCBDI), Shenzhen Institutes of Advanced Technology, Chinese Academy of Sciences, Shenzhen-Hong Kong Institute of Brain Science-Shenzhen Fundamental Research Institutions, Shenzhen 518055, China.
*These authors contributed equally to this work.
†Corresponding author. Email: shenwei@shanghaitech.edu.cn (W.L.S.); yangwen@shanghaitech.edu.cn (W.Z.Y.)
‡Present address: The MOE Frontier Science Center for Brain Research and Brain-Machine Integration, Zhejiang University School of Brain Science and Brain Medicine, Hangzhou, China.

## RESULTS

### Dynamic changes in BAT thermogenesis and tail vasodilation during heat defenses

To quantify the changes of thermoregulation variables during heat defense, we monitored the core temperature ($T_{core}$, measured intraperitoneally) together with the surface temperature of interscapular BAT ($T_{iBAT}$) and tail skin ($T_{tail}$) after exposing mice to warm ambient temperatures ($T_a$). As expected, these variables changed quickly after switching the $T_a$ from RT (room temperature) (25°C) to different target $T_a$ ranging from 30° to 38°C (Fig. 1, A to D). The peak $T_{tail}$ changes for each temperature switch increased as the target $T_a$ raised (Fig. 1E), suggesting that the vasodilation power increases as $T_a$ increases (*34*). Noticeably, the raise of $T_{iBAT}$ lagged behind the increase of $T_{core}$ (Fig. 1, F to H), and it became more evident with rising $T_a$ (Fig. 1, F to H), suggesting the BAT thermogenesis is further inhibited as $T_a$ increases (*35*). Together, we reveal the dynamic changes of two variables during heat defense, activation of vasodilation, and inhibition of BAT thermogenesis.

### The LPB→POA circuitry harbors neurons for inhibiting BAT thermogenesis and activating vasodilation

To find the neural substrates encoding different heat defense variables, we focused on the LPB→POA circuitry in the thermoregulatory reflex pathway. The LPB contains mostly glutamatergic neurons (*12*, *24*). To directly test their roles in thermoregulation, we used optogenetics to activate these glutamatergic neurons by targeted expression ChIEF, a current-stabilized channelrhodopsin (*36*), into the LPB of Vglut2-IRES-Cre mice (fig. S1, A to C). Photoactivation of these neurons led to unstable phenotypes. It caused either hypothermia or hyperthermia depending on stimulating laser frequencies (fig. S1D), suggesting activation of mixed cell types (*12*, *13*, *24*). Then, we photoactivated the LPB$^{Vglut2}$ terminals in the ventral medial POA

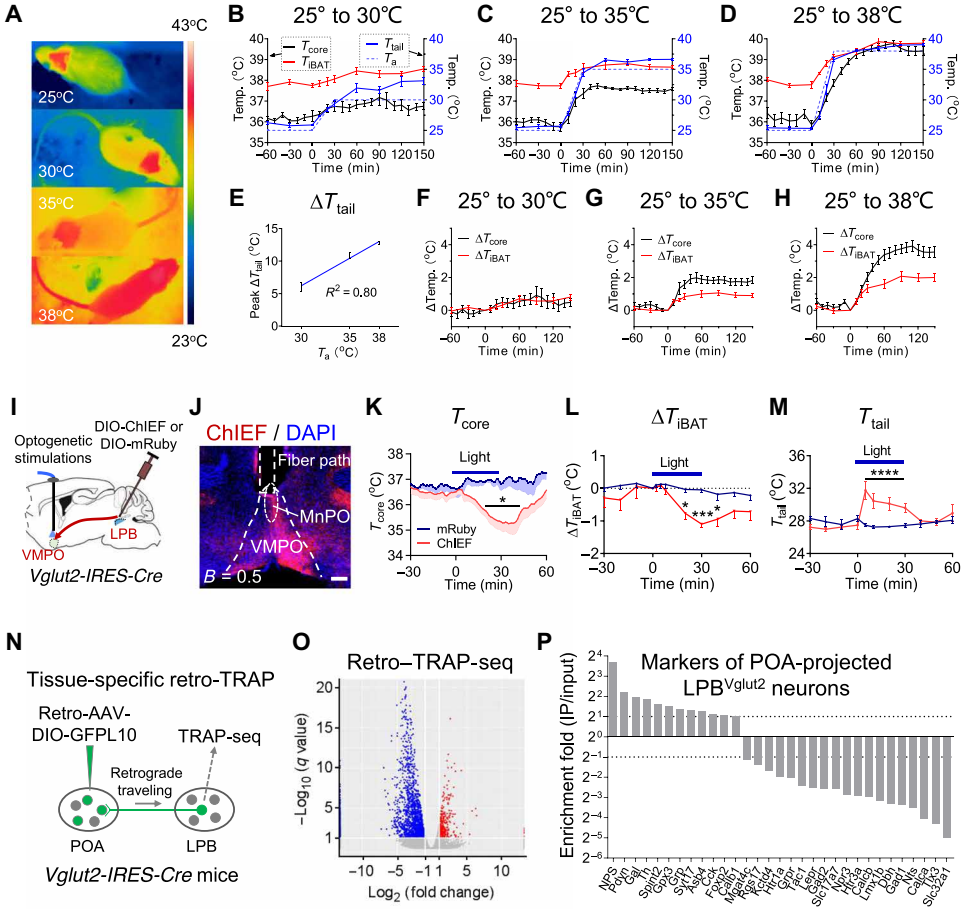


**Fig. 1. Heat defense variables and projection-specific analysis of the LPB→POA pathway.** (**A** to **D**) Changes of $T_{core}$, $T_{iBAT}$, and $T_{tail}$ under different ambient temperatures ($T_a$) ($n = 8$ each). (**E**) Peak $\Delta T_{tail}$ for different switches of ambient temperatures ($T_a$) ($n = 8$ each). The target $T_a$ was indicated. $\Delta T_{tail}$, $\Delta T_{core}$, and $\Delta T_{iBAT}$ are their current values subtracted by the value at $t = 0$. (**F** to **H**) Dynamics of $\Delta T_{core}$ and $\Delta T_{iBAT}$ over time under different $T_a$ switches ($n = 8$ each). (**I**) Scheme of optogenetic activation of glutamatergic (Vglut2) LPB terminals in the ventral medial POA (VMPO). (**J**) Expression of ChIEF from LPB$^{Vglut2}$ neural terminal in the VMPO. (**K** to **M**) Changes of $T_{core}$ (K), $\Delta T_{iBAT}$ (L), and $T_{tail}$ (M) after photoactivation LPB$^{Vglut2}$ terminals in the VMPO ($n = 4$ each). Laser pattern: 473 nm, 6 mW, 20 Hz, 10 ms, 2-s on after 2-s off, 30 min. (**N**) Scheme of tissue-specific retro-TRAP, where translational ribosomes from VMPO-projected LPB$^{Vglut2}$ neurons were immunoprecipitated and associated mRNAs were used for sequencing. (**O**) Volcano plots ($q$ value versus $\log_2$ fold change) for LPB mRNAs after retro-TRAP sequencing. Logarithmic ratios of mRNA enrichment fold (IP/Input, $n = 3$) plotted against the $q$ value (where $q \leq 0.5$ is considered significant) of the hierarchical linear model. Positive fold changes indicate an enrichment, and negative fold changes indicate a depletion in precipitated mRNAs. (**P**) Enrichment fold (IP/Input) of PB-expressed genes from Allen Institute. Scale bar, 200 μm. All data are shown as means ± SEM. All $P$ values are calculated on the basis of repeated measures two-way analysis of variance (ANOVA) with Bonferroni's corrections. *$P \leq 0.05$, ***$P \leq 0.001$, and ****$P \leq 0.0001$. B, bregma; scp, superior cerebellar peduncle; MnPO, median preoptic nucleus; VMPO, ventromedial preoptic nucleus.

(VMPO) and found that it only induced hypothermia (Fig. 1, I to K, and fig. S1E). Concurrently, it caused a reduction in $T_{iBAT}$ (Fig. 1L) and an increase in $T_{tail}$ (Fig. 1M), suggesting inhibition in BAT thermogenesis and activation in tail vasodilation.

Furthermore, to verify that POA neurons are the direct postsynaptic targets of LPB neurons, we activated VMPO neurons innervated by LPB neurons by using an anterograde transsynaptic tracer adeno-associated virus serotype 1 (AAV1)–Cre (*37*) injected into the LPB. This tracer induced expression of DIO-hM3D$_q$ injected into the VMPO, and these VMPO$^{hM3Dq}$ neurons were mainly glutamatergic as confirmed by glutamate staining (fig. S1, F and G). As expected, Designer receptors exclusively activated by designer drugs (DREADDs) activation of these VMPO neurons reduced $T_{core}$, EE, and physical activity (fig. S1, H to K), further supporting the role of this connection in thermoregulation. Thus, our data suggest the glutamatergic LPB→VMPO circuitry harbors neurons for inhibiting BAT thermogenesis and activating vasodilation.

## Transcriptome profiling of the LPB$^{Vglut2}$→POA circuitry

The finding that the LPB$^{Vglut2}$→VMPO circuitry controls heat defense variables prompts whether we could identify the underlying genetic substrates. To do this, we adopted a cell type– and projection-specific translating ribosome affinity purification (TRAP) based on a retrograde AAV (*38*). We injected a retro-AAV carrying DIO-GFP-L10 transgene (L10 is a ribosomal protein) (*39*) into the VMPO of the Vglut2-IRES-Cre mice, which expressed green fluorescent protein (GFP)–L10 in the LPB (Fig. 1N). First, we confirmed that warm-induced cFos colocalized with the GFP-L10 fluorescence in the LPB (fig. S1L). The GFP-labeled ribosomes were immunoprecipitated (IP) by anti-GFP antibodies after the LPB microdissection, and the associated mRNAs were collected for sequencing. We analyzed the enrichment fold IP/input and found that 364 genes were notably up-regulated and 1958 genes were down-regulated (Fig. 1O). Then, we focused on the enrichment fold of Parabrachial nucleus (PB)–expressed genes downloaded from Allen Institute (https://alleninstitute.org/) and found that up-regulated genes included neuropeptide S (*nps*), prodynorphin (*Pdyn*), galanin (*gal*), tyrosine hydroxylase (*th*), *CCK*, and *FoxP2*. The top down-regulated genes included GABAergic markers *Gad1* and *Slc32a1* and *LepR* (Fig. 1P). We chose these markers for further studies.

## Screening candidate markers for heat defense neurons in the LPB

We then analyzed the colabeling between temperature-induced cFos and genetic markers found in retro-TRAP experiment. NPS expressed broadly in the LPB, which colocalized with cFos induced by both heat exposure (~90%) and cold exposure (~88%) without an apparent selectivity (fig. S2, A and B). We took advantage of Pdyn-IRES-Cre mouse line and found Cre$^+$ neurons largely overlapped with Pdyn (~87%) and glutamate staining (~92%) (Fig. 2, A and B). Moreover, it labeled only ~20% of cFos$^+$ neurons induced by cold exposure and ~45% of cFos$^+$ neurons induced by heat exposure (Fig. 2, C and D), indicating a selectivity toward heat-activated neurons (*24*). More Pdyn$^+$ neurons were recruited when exposed to higher $T_a$, which ratiometrically matched the increases of cFos$^+$ neurons (Fig. 2, D to F). Therefore, the ratio of double-positive neurons (Pdyn$^+$ and cFos$^+$) over total cFos$^+$ neurons (double-positive/cFos$^+$) stayed constant (Fig. 2F).

Like Pdyn, more CCK-IRES-Cre$^+$ neurons were recruited when exposed to higher $T_a$ (Fig. 2, G to I). However, the recruited CCK$^+$ neurons exceeded the increases of cFos$^+$ neurons (Fig. 2, G to I). Therefore, the ratio of double-positive neurons (CCK$^+$ and cFos$^+$) over total cFos$^+$ neurons (double-positive/cFos$^+$) increased as the $T_a$ increased (Fig. 2I). The ratio of double-positive neurons over cFos$^+$ neurons induced by cold exposure was only ~20% (Fig. 2J), suggesting a selective response to heat exposure as well. Also, most CCK neurons were glutamatergic, as suggested by glutamate immunostaining (Fig. 2K). Furthermore, we checked the overlapping between Dynorphin A and CCK and found little overlapping (Fig. 2L), suggesting Pdyn$^+$ and CCK$^+$ neurons are separate populations.

To our surprise, there were few Gal-Cre$^+$ and TH$^+$ neurons in the LPB (fig. S2, C and D). Instead, we found a cluster of Gal-Cre$^+$ neurons in the laterodorsal tegmental nucleus and the locus coeruleus (fig. S2C) and a cluster of TH$^+$ neurons in the locus coeruleus (fig. S2D). Their enrichment might presumably be due to tissue contamination from nearby areas. Nevertheless, we also analyzed the overlapping between temperature-induced cFos and Gad1$^+$ cells and found few Gad1$^+$ cells in the LPB, which showed nearly no overlapping with cFos (fig. S2, E and F). Also, DREADD activation of LPB GABAergic neurons labeled by Vgat-IRES-Cre did not change $T_{core}$ significantly (fig. S2, G to I). DREADD activation of LepR-Cre neurons slightly increased $T_{core}$ (fig. S2, J to L). Together, we identified two types of LPB neurons, Pdyn and CCK neurons, as candidates for heat defense neurons based on their warm-selective responses.

## Neural dynamics of LPB$^{Pdyn/CCK}$→POA circuits to temperature changes

To further test the function of candidate heat defense neurons, we sought to record their responses to temperature stimuli. Therefore, we performed fiber photometry to record the LPB$^{Pdyn}$ calcium dynamics using GCaMP6s (Fig. 3, A and B). As expected, we observed a sustained calcium activity in response to floor warming (Fig. 3C), but only a small and quickly adapted response to floor cooling (Fig. 3D). The warming-induced responses showed little adaptation over a 10-min recording window and recovered to baseline after the temperature recovery (Fig. 3E). Fitting the peak responses to various warm floor temperatures revealed a linear relationship between calcium levels and floor temperatures (Fig. 3, F and G). Next, we recorded the calcium activity from VMPO terminals of LPB$^{Pdyn}$ neurons and also found a sustained response to warming (Fig. 3, H to J). In contrast to the soma, we did not detect any significant changes to cooling (Fig. 3K), suggesting that the activity of this projection is warm specific. Also, we measured responses to other stimuli, including the novel object, chow, HFD, and mouse and found no significant changes to these stimuli (Fig. 3L).

Under the same experimental settings, we recorded jGCaMP7b signals from CCK-Cre mice. We found that both the LPB$^{CCK}$ soma and their terminals in the VMPO selectively responded to warming than the cooling (Fig. 3, M to U). Similar to LPB$^{Pdyn}$ soma, fitting the peak responses of the LPB$^{CCK}$ soma signals to various warm floor temperatures revealed a linear relationship between calcium levels and temperatures (Fig. 3, P and Q). Together, we showed that LPB$^{Pdyn/CCK}$→POA circuits are selectively sensitive to warming, and the responses are linearly increased as the increase of floor temperatures.

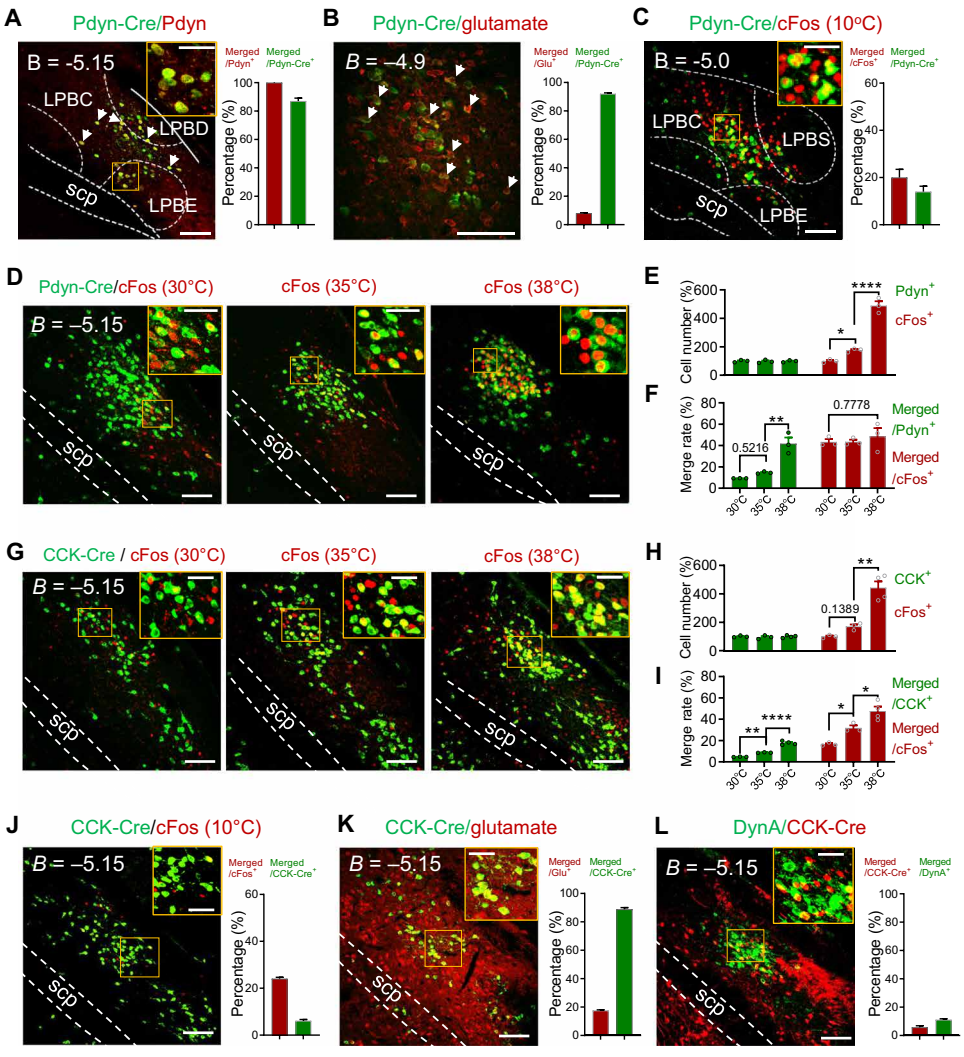


**Fig. 2. LPB$^{Pdyn/CCK}$ neurons are candidate heat defense neurons.** (**A**) The overlapping between Pdyn-IRES-Cre and AAV-DIO-GFP and Pdyn staining in the LPB ($n = 3$ each). Arrows, examples of merged cells. (**B**) The overlapping between Pdyn-Cre and LSL-GFPL10 and glutamate staining in the LPB ($n = 3$ each). (**C**) The overlapping between Pdyn-Cre and LSL-GFPL10 and cold-induced cFos (10°C) in the LPB ($n = 3$ each). (**D** to **F**) The overlapping between Pdyn-Cre and LSL-GFPL10 and cFos induced by different warm ambient temperatures as indicated. Representative images are shown in [(D); $n = 3$ each). The relative cell numbers are shown in [(E) normalized to 30°C] and merge rates are shown in (F). (**G** to **I**) The overlapping between CCK-IRES-Cre and LSL-GFPL10 and cFos induced by different ambient temperatures as indicated. Representative images are shown in [(G); $n \geq 3$ each]. The relative cell numbers are shown in [(H) normalized to 30°C] and merge rates are shown in (I). (**J**) The overlapping between CCK-Cre and LSL-GFPL10 and cold-induced cFos (10°C) in the LPB ($n = 3$ each). (**K**) The overlapping between CCK-Cre and LSL-GFPL10 and glutamate staining in the LPB ($n = 3$ each). (**L**) The overlapping between CCK-Cre and LSL-GFPL10 and DynA staining in the LPB ($n = 3$ each). Scale bars, 100 μm except in upper right boxes (50 μm). All data are shown as means ± SEM. All the $P$ values are calculated based on ordinary one-way ANOVA with Tukey's corrections. *$P \leq 0.05$, **$P \leq 0.01$, and ****$P \leq 0.0001$. LPBC, LPB central part; LPBD, LPB dorsal part; LPBS, LPB superior part; LPBE, LPB external part.

## Monosynaptic connections between LPB$^{Pdyn/CCK}$ neurons and POA neurons

The sensitivity of LPB$^{Pdyn/CCK}$→POA projections to warmth motivated us to test whether there was a direct connection between LPB$^{Pdyn/CCK}$ neurons and POA neurons. Thus, we first recorded the light-induced excitatory postsynaptic currents (EPSCs) from VMPO neurons in LPB$^{Pdyn\&ChIEF}$ mice. These currents were blocked by glutamate receptor antagonists CNQX/AP5 (Fig. 4, A and B), supporting the nature of glutamatergic transmission. To test whether it was a monosynaptic connection, we first blocked the EPSCs with tetrodotoxin (TTX) and then applied 4-aminopyridine (4-AP) to sensitize the postsynaptic current. We found that the EPSCs were recovered by 4-AP, suggesting that LPB$^{Pdyn}$ neurons and VMPO neurons form a monosynaptic connection (Fig. 4C). Similarly, LPB$^{CCK}$ neurons also formed glutamatergic monosynaptic connections with VMPO neurons (Fig. 4, D to F).

## LPB$^{Pdyn/CCK}$→POA circuits are sufficient to induce hypothermia

The neural activity and direct connections within the LPB$^{Pdyn/CCK}$→POA circuits suggested a functionally important pathway in heat defense. To test the hypothesis, we used DREADD-hM3D$_q$ to activate their

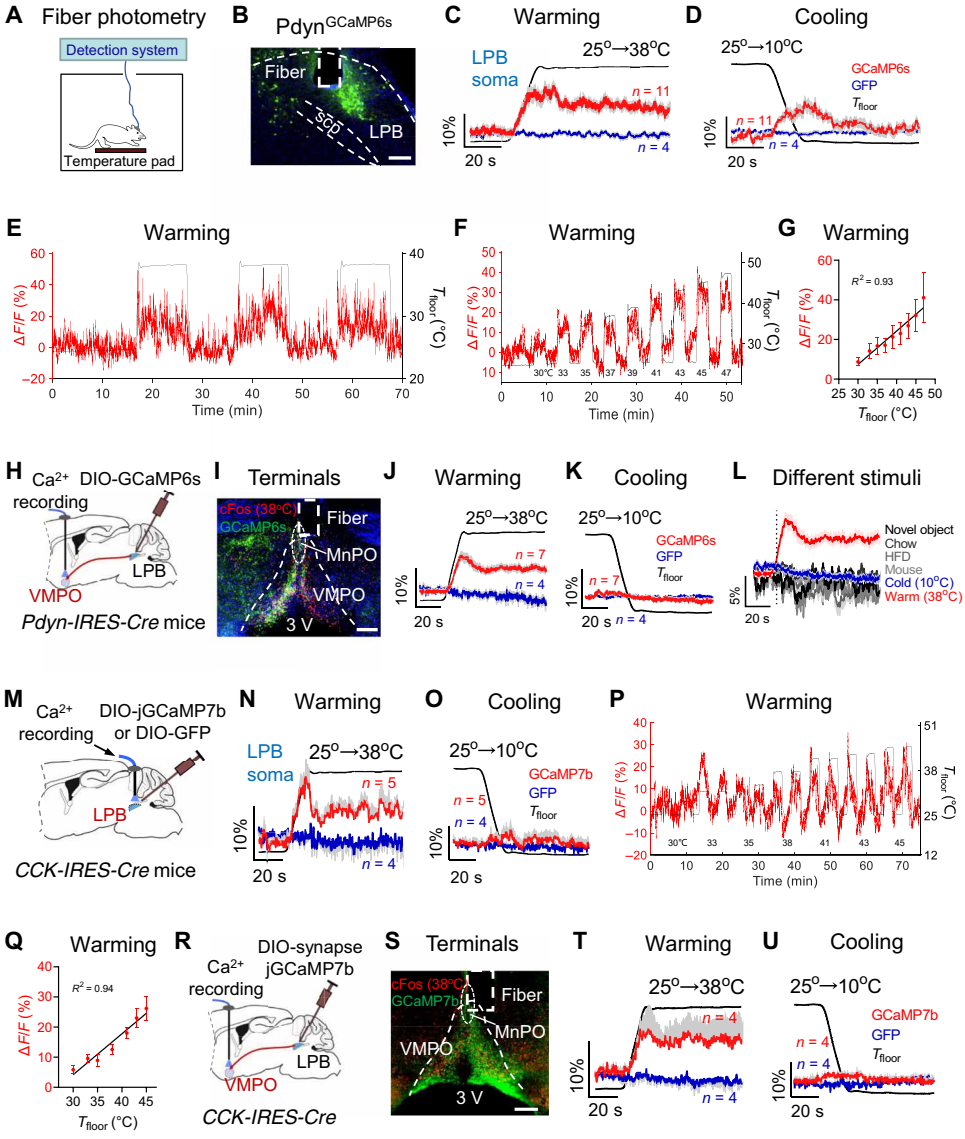


**Fig. 3. LPB$^{Pdyn/CCK}$→POA circuitry is sensitive to warm temperatures.** (**A**) Scheme of $Ca^{2+}$ fiber photometry. The floor temperature ($T_{floor}$) was controlled by a Peltier device. (**B**) Expression of DIO-GCaMP6s in LPB$^{Pdyn}$ neurons. (**C** and **D**) Calcium dynamics from LPB$^{Pdyn}$ soma after warming (C) or cooling (D) of the floor. $\Delta F/F_0$ represents the change in GCaMP6s fluorescence from the mean level [$t$ = (−120 to 0 s)] [as to (**J**), (**K**), (**L**), (**N**), (**O**), (**T**), and (**U**)]. The GFP was used as a control. (**E**) A representative trace of LPB$^{Pdyn}$ soma to a 10-min warm stimuli. (**F** and **G**) A representative trace of LPB$^{Pdyn}$ soma to different $T_{floor}$ (F) and the correlation between peak $\Delta F/F_0$ and floor temperatures (G) ($n$ = 5). (**H**) Scheme for calcium recording of LPB$^{Pdyn}$ terminals in the VMPO. (**I**) Expression of DIO-GCaMP6s from LPB$^{Pdyn}$ neural terminals in the VMPO and warm-induced cFos. (J and K) Calcium dynamics from LPB$^{Pdyn}$ neural terminals in the VMPO after warming (J) or cooling (K), respectively. (L) Summary of responses from LPB$^{Pdyn}$ neural terminals in the VMPO to indicated stimuli, including novel objects, chow food, HFD, mouse of the same sex, and temperatures ($n$ = 4 each). (**M**) Scheme for soma recording of calcium signals in LPB$^{CCK}$ neurons. (N and O) Calcium dynamics from LPB$^{CCK}$ soma after warming (N) or cooling (O) of the floor, respectively. (**P** and **Q**) A representative trace of LPB$^{CCK}$ soma to different floor temperatures (P) and the correlation between peak $\Delta F/F_0$ and floor temperatures (Q) ($n$ = 6). (**R**) Scheme for calcium recording of LPB$^{CCK}$ neural terminals in the VMPO. (**S**) Expression of DIO-synapse-jGCaMP7b from LPB$^{CCK}$ terminals in the VMPO and warm-induced cFos. (T and U) Calcium dynamics from LPB$^{CCK}$ terminals in the VMPO after warming (T) or cooling (U) of the floor, respectively. Scale bars, 200 μm. All data are shown as means ± SEM.

somata in the LPB. As expected, activation of LPB$^{Pdyn}$ soma lowered $T_{core}$, EE, and physical activity (fig. S3, A to F) yet did not affect $T_{tail}$ (fig. S3G). The reduction of $T_{core}$ and EE was reversed by injection of adrenergic β3 agonist CL316243 (fig. S3, H and I). It reduced food intake in fed state, but not in fasted state (fig. S3, J and K), which is consistent with its function in tension-induced feedback inhibition of food intake (*29*). Similarly, DREADD activation of LPB$^{CCK}$ soma reduced $T_{core}$, EE, and physical activity (fig. S3, L to P). Yet, it increased tail vasodilation as measured by $T_{tail}$ (fig. S3Q), suggesting that the two types of neurons regulate vasodilation differentially. It did not affect food intake in both the fed and fasted states (fig. S3, R and S). Also, it slightly and insignificantly reduced blood glucose level (fig. S3T), suggesting this is a separate population from the CCK$^+$ glucose up-regulation neurons (*30*, *31*).

Next, we photoactivated LPB$^{Pdyn\&ChIEF}$ neural terminals in the VMPO. Photoactivation of these terminals induced hypothermia

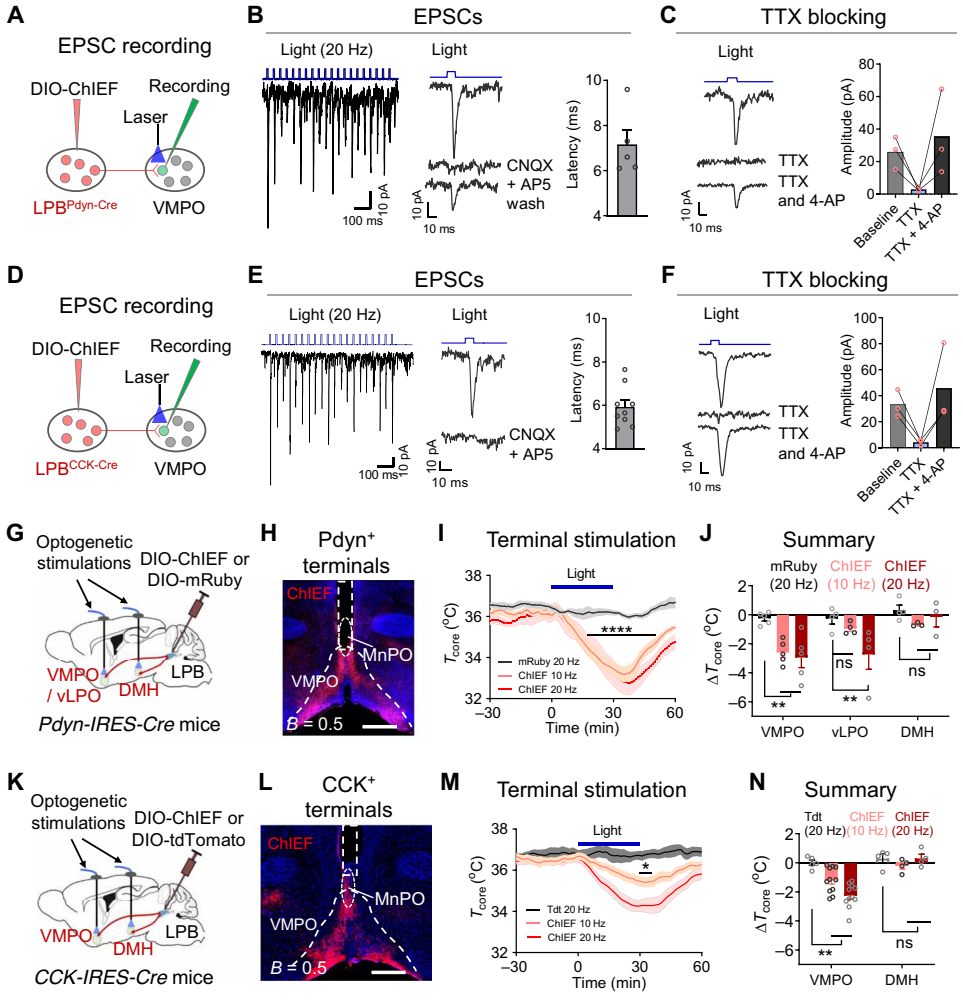


**Fig. 4. LPB$^{Pdyn/CCK}$→POA circuits induce hypothermia.** (**A** to **F**) Light-evoked EPSCs recorded from VMPO neurons innervated by LPB$^{Pdyn}$ (A to C) and LPB$^{CCK}$ (D to F) neurons. Light patterns: blue, 7 mW, 10 ms. EPSCs were blocked by GluR antagonists, AP5, and CNQX (B and E). EPSCs were blocked after TTX and were recovered by TTX and 4-AP treatment (C and F). (**G**) Scheme for optogenetic stimulation of LPB$^{Pdyn\&ChIEF}$ neural terminals. (**H**) The LPB$^{Pdyn\&ChIEF}$ neural terminals in the VMPO. (**I**) Changes of $T_{core}$ after photoactivation of LPB$^{Pdyn}$ neural terminals in the VMPO ($n = 5$ each). (**J**) Quantification of $\Delta T_{core}$ after photoactivation of LPB$^{Pdyn}$ terminals in the VMPO ($n = 5$ each), the vLPO ($n = 4$ each), and the DMH (mRuby, $n = 4$; ChIEF, $n = 3$). Laser pattern: 473 nm, 6 mW, Hz as indicated, 30 min. (**K**) Scheme for optogenetic stimulation of LPB$^{CCK\&ChIEF}$ terminals. (**L**) The LPB$^{CCK\&ChIEF}$ neural terminals in the VMPO. (**M**) Changes of $T_{core}$ after photoactivation of LPB$^{CCK}$ terminals in the VMPO. (**N**) Quantification of $\Delta T_{core}$ after photoactivation of LPB$^{CCK}$ terminals in the VMPO (tdTomato, $n = 5$; ChIEF, $n = 11$) and the DMH ($n = 4$ each). Laser pattern: 473 nm, 3 mW, 30 min. Scale bars, 500 μm. All data are shown as means ± SEM. The *P* values are calculated on the basis of repeated measures two-way ANOVA with Bonferroni's corrections (I and M) and ordinary two-way ANOVA with Dunnett's corrections (J and N). *$P \leq 0.05$, **$P \leq 0.01$, and ****$P \leq 0.0001$; ns, not significant. DMH, dorsomedial hypothalamus; vLPO, ventral part of lateral preoptic nucleus.

(Fig. 4, G to I, and fig. S4, A and B). Also, we found that a 5-Hz photostimulation was sufficient to induce significant hypothermia, and the level of hypothermia was saturated after 10-Hz photostimulation (Fig. 4I, and fig. S4B). Furthermore, we tested whether this induced hypothermia was sensitive to ambient temperatures and energy state. The induced hypothermia was reduced by warming in 30°C and was substantially suppressed after 24-hour fasting (fig. S4, C and D). The reduced hypothermia at 30°C might be due to reduced radiation loss, since the difference between $T_{core}$ and $T_a$ was reduced. Besides the VMPO, LPB$^{Pdyn}$ neurons send out projections to other regions, including the ventral part of the lateral preoptic nucleus (vLPO) and the dorsomedial hypothalamus (DMH) (fig. S4A). We also tested their functions by photoactivation. Unlike the stimulation in the VMPO, only a 20-Hz stimulation, not lower frequencies, could induce significant hypothermia in the vLPO (Fig. 4J and fig. S4, E to G). There were no changes in $T_{core}$ after activation of terminals in the DMH (Fig. 4J and fig. S4, H to J).

Like Pdyn$^+$ terminals, activation of CCK$^+$ terminals in the VMPO, but not in the DMH, caused hypothermia (Fig. 4, K to N, and fig. S5). Unlike Pdyn$^+$ terminals, the hypothermia induced by activation of CCK$^+$ terminals in the VMPO was not affected by warmth nor fasting (fig. S5, C and D), suggesting that the two circuits may function independently. There might be some compensatory mechanisms to limit radiation heat loss at RT when compared to hypothermia induced by Pdyn stimulation (figs. S4C and S5C). Together, these

results suggest that LPB$^{Pdyn/CCK}$→POA circuits are sufficient to reduce body temperature.

### Categorical regulation of heat defense variables by LPB$^{Pdyn/CCK}$→POA circuits

Heat defense variables include (at least) inhibition of thermogenesis and activation of vasodilation (Fig. 1). We suspected LPB$^{Pdyn/CCK}$ neurons would regulate these variables. Therefore, we recorded $T_{tail}$ and $T_{iBAT}$ during photoactivation of their terminals in the VMPO. We did not detect any changes in $T_{tail}$ after activation of Pdyn$^{+}$ terminals (Fig. 5, A to C). Substantially, we found a rapid decrease of $T_{iBAT}$ (with embedded probes), which appeared to precede the changes of $T_{core}$ (Fig. 5B). Also, it significantly reduced the cold-induced shivering electromyogram (EMG) activity and physical activity levels, although the reduction of physical activity occurred after stimulation (Fig. 5, D and E, and fig. S6, A to C). The observation that the $T_{iBAT}$ reduction appeared to precede the $T_{core}$ reduction hints that the lowered BAT thermogenesis might be a driver for the $T_{core}$ reduction. Yet, the time resolution was too low to tell the kinetics, since they were sequentially recorded by noncompatible wireless probes at low time resolution. Therefore, we made two pluggable wired thermocouples to simultaneously record $T_{core}$ and

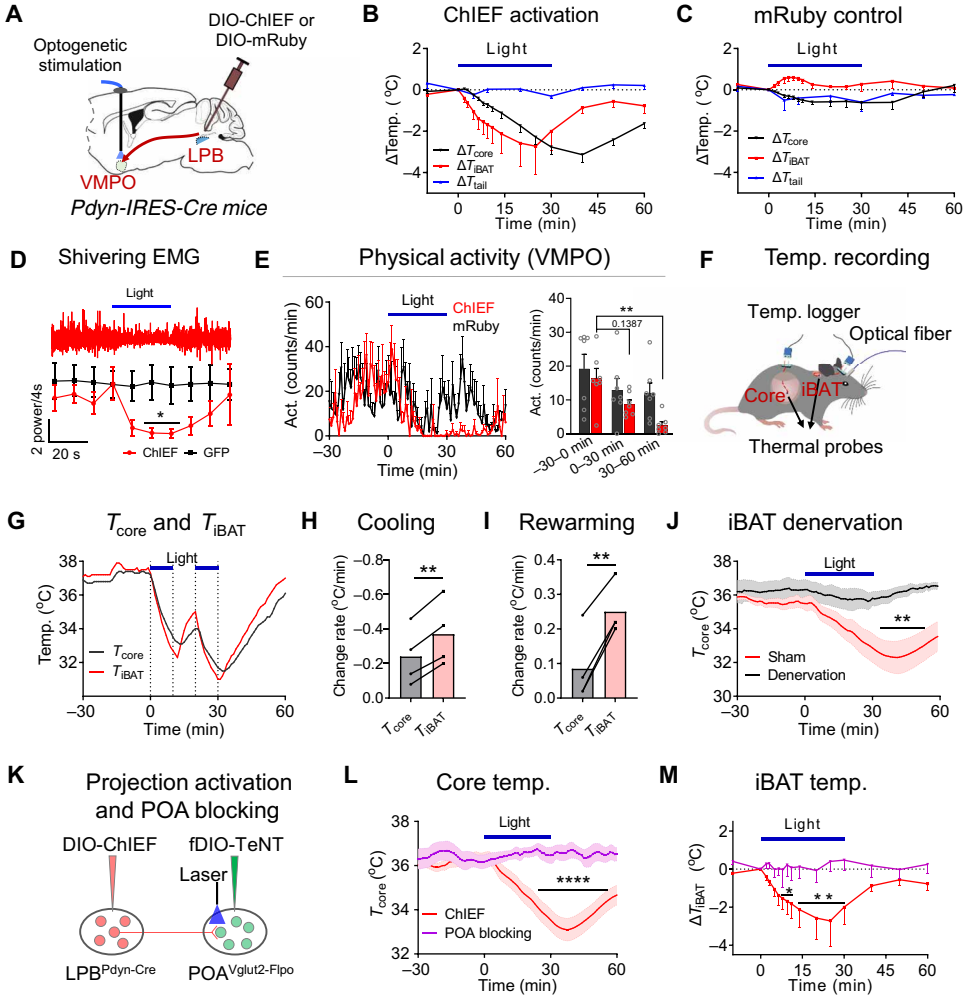


**Fig. 5. LPB$^{Pdyn}$→POA circuit regulates iBAT thermogenesis and muscle shivering.** (**A**) Scheme for optogenetic stimulation of LPB$^{Pdyn\&ChIEF}$ terminals in the VMPO (terminal photostimulation). (**B** and **C**) Dynamics of $\Delta T_{core}$, $\Delta T_{iBAT}$, and $\Delta T_{tail}$ after terminal photostimulation (B) ($n = 5$, 5, and 7, respectively) and controls (C) ($n = 4$ each). $\Delta T_{tail}$, $\Delta T_{core}$, and $\Delta T_{iBAT}$ are their current values subtracted by the value at t = 0. (**D**) Shivering EMG of the nuchal muscle after terminal photostimulation (ChIEF, $n = 5$; GFP, $n = 6$; $T_{skin} = 10$°C.). (**E**) Changes of physical activity after terminal photostimulation ($n = 7$ each). (**F**) Scheme for simultaneous recording of $T_{core}$ and $T_{iBAT}$ by pluggable T-type thermocouples. (**G** to **I**) Representative traces of $T_{core}$ and $T_{iBAT}$ after terminal photostimulation (G) and mean change rates (first 5 min) of $T_{core}$ and $T_{iBAT}$ during the phase of body cooling (H) and rewarming (I) ($n = 4$ each). (**J**) $T_{core}$ changes induced by terminal photostimulation in sham group and iBAT sympathetic nerves denervated group ($n = 4$ each). (**K**) Scheme to block POA glutamatergic neurons while photoactivation of LPB$^{Pdyn}$ neuron terminals in the VMPO. (**L** and **M**) POA glutamatergic blocking abolished the photoactivation-induced effect in $T_{core}$ reduction (L) (ChIEF replotted from Fig. 4I.) and $T_{iBAT}$ reduction (M) (ChIEF replotted from (B), POA blocking, $n = 4$. $\Delta T_{(t=i)} = T_{(t=i)} - T_{(t=0)}$, Laser patterns: 473 nm, 6 mW, 20 Hz, 2-s on after 2-s off, time as indicated. All data are shown as means ± SEM. The *P* values are calculated on the basis of repeated measures two-way ANOVA with Bonferroni's corrections (D, J, L, and M), ordinary two-way ANOVA with Bonferroni's corrections (E), and paired *t* tests (H and I). *$P \leq 0.05$, **$P \leq 0.01$, and ****$P \leq 0.0001$.

$T_{iBAT}$ at high temporal resolution (Fig. 5F). During body cooling, the $T_{iBAT}$ reduced before the $T_{core}$ and reached a lower value than $T_{core}$ (Fig. 5G). Conversely, during rewarming, $T_{iBAT}$ increased before the $T_{core,}$ and reached a higher value than $T_{core}$ (Fig. 5I). The changing rates of $T_{iBAT}$ were significantly larger than those of $T_{core}$ (Fig. 5, H and I). Thus, the kinetics supports that the change of iBAT thermogenesis is a driver of $T_{core}$ changes. Next, to directly test whether iBAT is required for $T_{core}$ changes, we denervated their sympathetic nerves. It did not affect basal temperatures when kept at 25°C (fig. S6F), yet it indeed blocked the hypothermia induced by photoactivation (Fig. 5J). Therefore, these data support that the reduction of BAT thermogenesis is the driver of $T_{core}$ reduction.

Next, we suspected that POA glutamatergic neurons might be the target of $LPB^{Pdyn}$ neurons, since we showed that LPB-innervated POA neurons were mainly glutamatergic (fig. S1, F and G) and that POA glutamatergic neurons can induce hypothermia (*16*, *18*, *20*). To test it, we made a Vglut2-2A-Flpo mouse line so that we could simultaneously modulate the activities of $LPB^{Pdyn}$ neurons and $POA^{Vglut2}$ neurons using Cre/Loxp and Flpo/Frt systems, respectively. We validated the Flpo expression in the hypothalamus (fig. S6, G to J) and verified its function in blocking warm- and cold-induced thermoregulation in the POA using tetanus neurotoxin (TeNT) (fig. S6, K and L). Then, we blocked $POA^{Vglut2\text{-}Flpo}$ neurons with TeNT while photoactivating $LPB^{Pdyn}$ terminals in the VMPO (Fig. 5K). As expected, this blocking abolished the reduction of $T_{core}$ and $T_{iBAT}$ induced by terminal activation (Fig. 5, L and M). In contrast, blocking LepR neurons in the VMPO did not affect the hypothermia induced by the $Pdyn^+$ terminal activation (fig. S7, A to C). Therefore, our data suggest that the $LPB^{Pdyn}\rightarrow POA^{Vglut2}$ circuit inhibits iBAT thermogenesis to reduce body temperature.

Using similar methods, we found that activation of $LPB^{CCK}$ terminals in the VMPO markedly increased the $T_{tail}$ (Fig. 6, A to C), suggesting that this projection is a potent activator of vasodilation. It also reduced $T_{iBAT}$, yet the kinetics of $T_{iBAT}$ changes was indistinguishable to the changes of $T_{core}$ (Fig. 6B), which led us to suspect that the reduction of $T_{iBAT}$ is a secondary effect of $T_{core}$ reduction. Therefore, we denervated their sympathetic nerves and found that it indeed did not affect the induced hypothermia (Fig. 6D), suggesting that iBAT function was not required. The changes of $T_{iBAT}$ were probably a secondary effect due to body cooling (Fig. 6B). Furthermore, unlike the partial blocking of shivering EMG seen after $Pdyn^+$ terminal activation (Fig. 5D), activation of $LPB^{CCK}$ terminals in the VMPO completely suppressed the shivering EMG activity (Fig. 6E and fig. S6, D and E). Also, like Pdyn stimulation, it reduced physical activity only after photostimulation (Fig. 6F).

Nevertheless, we checked whether the nucleus of the solitary tract (NTS), the baroreflex control center (*40*), would provide inputs to the LPB to modulate vasodilation. Activation of glutamatergic NTS→LPB pathway indeed induced hypothermia but did not affect tail vasodilation (fig. S7, D to J), suggesting that this connection might be dispensable for vasodilation. Together, our data define LPB $Pdyn^+$ and $CCK^+$ neurons function via their POA projections to categorically regulate the inhibition of iBAT thermogenesis and the activation of vasodilation, respectively, and to differentially regulate cold-induced muscle shivering.

### $LPB^{Pdyn}\rightarrow$POA circuit is required for inhibition of BAT thermogenesis during heat defense, fever limiting, and body weight control

The finding that LPB neuron types could regulate heat defense variables hints that they might be required for heat defense. To test

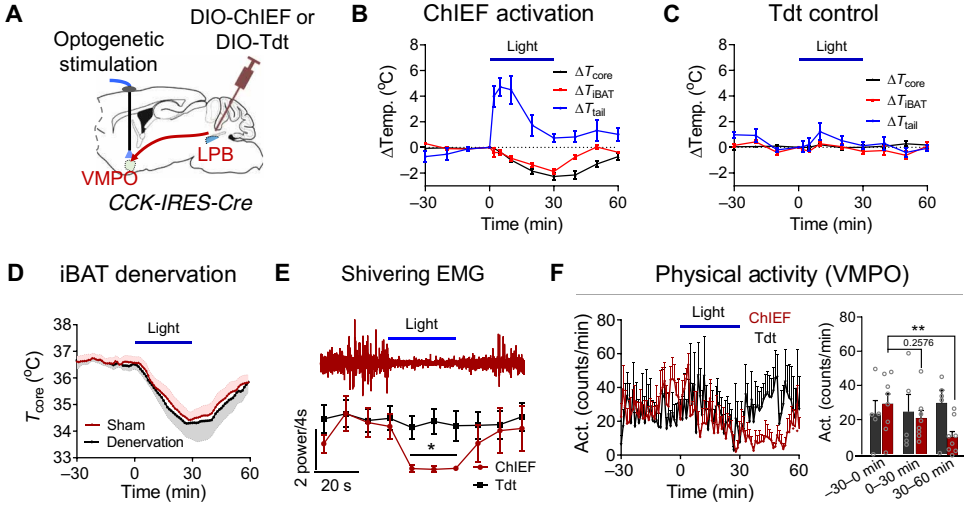


**Fig. 6. $LPB^{CCK}\rightarrow$POA circuit regulates vasodilation and muscle shivering.** (**A**) Scheme for optogenetic stimulation of $LPB^{CCK\&ChIEF}$ terminals in the VMPO. (**B** and **C**) Dynamics of $\Delta T_{core}$, $\Delta T_{iBAT}$, and $\Delta T_{tail}$ after photoactivation of $LPB^{CCK}$ terminals in the VMPO (B) ($n = 11$, 5, and 6, respectively) and controls are shown in (C) ($n = 4$ each). $\Delta T_{core}$, $\Delta T_{iBAT}$, and $\Delta T_{tail}$ are the values of $T_{core}$, $T_{iBAT}$, and $T_{tail}$ subtracted by the value at t = 0, respectively. (**D**) $T_{core}$ changes induced by photoactivation of $LPB^{CCK}$ terminals in the VMPO in the sham group and iBAT sympathetic nerves denervated group ($n = 8$ each). (**E**) Shivering EMG of the nuchal muscle after photoactivation of $LPB^{CCK}$ terminals in the VMPO (ChIEF, $n = 4$; tdTomato, $n = 6$). (**F**) Changes of physical activity after photoactivation of $LPB^{CCK}$ terminals in the VMPO (ChIEF, $n = 8$; tdTomato, $n = 5$). Laser patterns: 473 nm, 6 mW [3 mW in (D)], 20 Hz, 2-s on after 2-s off, time as indicated. (−30 to 0 min), (0 to 30 min), and (30 to 60 min) in (F) represents the averaged physical activity between $t = (-30$ to 0 min), $t = (0$ to 30 min), and $t = (30$ to 60 min), respectively. All data are shown as means ± SEM. The *P* values are calculated on the basis of repeated measures two-way ANOVA with Bonferroni's corrections (E) and ordinary two-way ANOVA with Bonferroni's corrections (right panels in F). $^*P \leq 0.05$, $^{**}P \leq 0.01$.

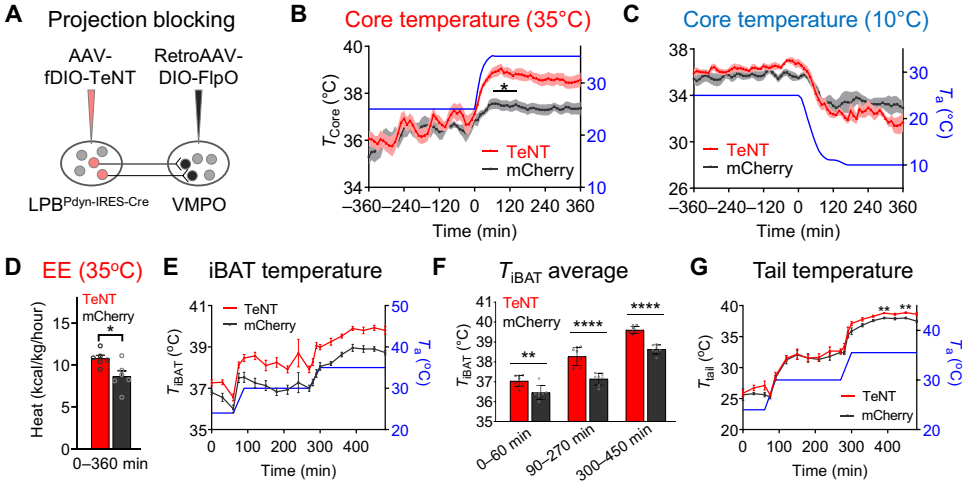


**Fig. 7. LPB$^{Pdyn}$→POA circuit is required for heat defense.** (**A**) Scheme for blocking POA-projected LPB$^{Pdyn}$ neurons using neurotoxin TeNT. Retrograde AAVs carrying Cre-dependent FlpO were injected in the VMPO, which drives expression of FlpO-dependent TeNT in the LPB. (**B** and **C**) Changes of $T_{core}$ after warm (B) and cold (C) exposures, respectively ($n = 6$ each), where mCherry is the control. (**D**) Changes of EE after warm exposure ($n = 6$ each). (0 to 360 min) represents the averaged EE between $t = (0$ to 360 min). (**E** and **F**) Changes of $T_{iBAT}$ (E) and their quantification (F) under different ambient temperatures ($T_a$) recorded by an infrared camera (TeNT, $n = 8$; mCherry, $n = 7$). The coat hair on top of the iBAT was shaved. (0 to 60 min), (90 to 270 min), and (300 to 450 min) in (F) represent the averaged $T_{iBAT}$ between $t = (0$ to 60 min), $t = (90$ to 270 min), and $t = (300$ to 450 min), respectively. (**G**) Changes of $T_{tail}$ under different $T_a$ recorded by an infrared camera (TeNT, $n = 8$; mCherry, $n = 7$). All data are shown as means ± SEM. The $P$ values are calculated on the basis of repeated measures two-way ANOVA with Bonferroni's corrections (B, C, and G), ordinary two-way ANOVA with Bonferroni's corrections (F), and unpaired $t$ tests (D). *$P \leq 0.05$, **$P \leq 0.01$, and ****$P \leq 0.0001$.

this, we blocked POA-projected LPB$^{Pdyn}$ neurons by targeted expression of TeNT in this circuit (Fig. 7A). Blocking these Pdyn neurons elevated the basal body temperature and EE, but not physical activity (fig. S8, A to C). As expected, this blocking impaired thermoregulation after warm exposure (35°C), with a much higher $T_{core}$ than the control (Fig. 7B). In contrast, there was only a small and insignificant effect on the $T_{core}$ after cold exposure (Fig. 7C), suggesting that this blocking selectively affects heat defense. Consistent with $T_{core}$ changes, the neural blocking caused slightly and significantly elevated EE in warm temperature, but not in cold temperature (Fig. 7D and fig. S8, D and E). No significant changes were found in physical activity in warm and cold temperatures (fig. S8, F and G).

We suspected that the POA-projected Pdyn neural blocking would increase iBAT thermogenesis as their activation inhibits it (Fig. 5B). Thus, we measured $T_{iBAT}$ and found that $T_{iBAT}$ was elevated remarkably in both RT and warm temperatures (Fig. 7, E and F), which indicates disinhibition in iBAT thermogenesis and provides an explanation for the increases in basal body temperature and EE. The $T_{tail}$ was elevated only at the delayed stage after warm exposure when compared to controls (Fig. 7G), which presumably was due to the elevated $T_{core}$.

The increased EE after blocking POA-projected LPB$^{Pdyn}$ neurons prompted us to test whether broadly blocking LPB$^{Pdyn}$ neurons would have a more substantial effect in disinhibiting EE, thereby affecting body weights. We found a profound elevation in basal $T_{core}$ and EE after broadly blocking LPB$^{Pdyn}$ neurons with TeNT (fig. S9, A to C). The basal physical activity and food intake were not affected (fig. S9, D and E). Similarly, it impaired thermoregulation after warm exposure, but not after cold exposure (fig. S9, F and G). As expected, it caused a substantial increase of $T_{iBAT}$ at RT or in warm temperatures (fig. S9H) and aggravated fever induced by interleukin-1β (IL-1β) injection [intraperitoneal (i.p.)] (fig. S9I). Then, we measured body weight changes under chow or HFD and found that it significantly limited the body weight gain driven by HFD without changing the amount of HFD intake (fig. S9, J and K). Moreover, we tested the behavioral preference to warm and cold temperatures and found that it increased the warm preference significantly, but not the cold preference (fig. S9, L and M), suggesting an altered behavioral propensity toward increasing $T_{core}$. Together, we establish that the LPB$^{Pdyn}$→POA circuit encodes the inhibition of iBAT thermogenesis in heat defense, limits fever, promotes warm preference, and regulates EE and body weight.

## LPB$^{CCK}$→POA circuit is required for vasodilation during heat defense and fever limiting

To test the necessity of the CCK circuitry in heat defense, we blocked POA-projected LPB$^{CCK}$ neurons by targeted expression of TeNT (Fig. 8A). Like Pdyn neural blocking, it selectively impaired thermoregulation after warm exposure, with a much higher $T_{core}$ than the control (Fig. 8, B and C). This blocking also aggravated fever induced by IL-1β (Fig. 8D). However, unlike Pdyn neural blocking, it did not affect basal $T_{core}$ and EE (fig. S10, A and B) and did not significantly increase $T_{iBAT}$ when compared to the control until the $T_a$ was very high (35°C) (Fig. 8, E and F). The delayed increase of $T_{iBAT}$ at 35°C was presumably due to the elevated $T_{core}$ (Fig. 8, B and E). Moreover, it did not affect basal physical activity, body weight, and EE and physical activity after warm and cold exposures (fig. S10, C to H). The increase of $T_{tail}$ was significantly delayed when switching the $T_a$ from 30° to 35°C as compared to controls (Fig. 8G), suggesting that tail vasodilation was impaired. To see a more significant defect in vasodilation, we increased the changes of $T_a$ by switching from 25° to

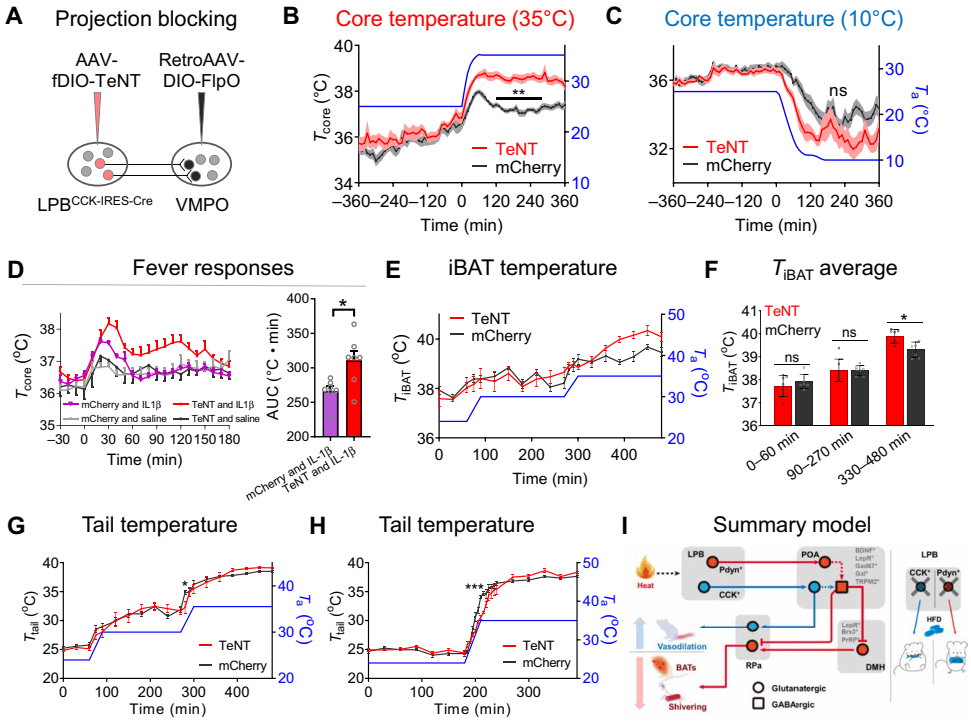


**Fig. 8. LPB$^{CCK}$→POA circuit is required for heat defense and fever limiting.** (**A**) Scheme for blocking POA-projected LPB$^{CCK}$ neurons using TeNT. (**B** and **C**) Changes of $T_{core}$ after warm (B) and cold (C) exposures, respectively (TeNT, $n = 7$; mCherry, $n = 8$). (**D**) Fever responses after injection of IL-1β ($n = 7$ each group; 10 to 12 weeks after viral injection). AUC, area under the curve. (**E** and **F**) Changes of $T_{iBAT}$ (E) and their quantification (F) under different $T_a$ ($n = 7$ each). (0 to 60 min), (90 to 270 min), and (330 to 480 min) in (F) represent the averaged $T_{iBAT}$ between $t =$ (0 to 60 min), $t =$ (90 to 270 min), and $t =$ (330 to 480 min), respectively. (**G** and **H**) Changes of $T_{tail}$ under different $T_a$ ($n = 7$ each). (**I**) Proposed model for LPB$^{Pdyn/CCK}$ circuits in regulating iBAT thermogenesis, vasodilation, muscle shivering, and body weight. All data are shown as means ± SEM. The *P* values are calculated on the basis of repeated measures two-way ANOVA with Bonferroni's corrections (B, C, G, and H), ordinary two-way ANOVA with Bonferroni's corrections (F), and unpaired *t* tests (D). $^*P \leq 0.05$, $^{**}P \leq 0.01$, and $^{***}P \leq 0.001$.

35°C. As expected, we found a more substantial delay in $T_{tail}$ increase (Fig. 8H). Together, we show that the LPB$^{CCK}$→POA circuit encodes tail vasodilation during heat defense and limits fever development.

## DISCUSSION

### Roles of the LPB in thermoregulation

The LPB has been proposed as a relay center to transmit "feed-forward" thermosensory signals into the POA, the thermoregulation center (*6*). Whether the LPB is actively involved in processing warm sensory signals is unknown, and the genetic identity of LPB thermoregulatory neurons remains poorly characterized. By transcriptome analysis, activity recordings, and functional manipulations, we genetically define two subsets of LPB glutamatergic neurons, the Pdyn and CCK neurons, as thermoregulatory neurons for autonomic responses to heat defense and fever limiting. By finding that Pdyn and CCK neurons categorically encode inhibition of thermogenesis and activation of vasodilation, respectively, and differentially inhibit muscle shivering, we suggest that the LPB is a critical center early in the thermoreflex pathway to segregate warm afferent signals that lastly leads to differential regulation of peripheral targets.

### BAT thermogenesis links thermoregulation to body weight control

The neural substrates for temperature-induced adaptive thermogenesis remain to be better explored (*5*, *6*), and the integration between thermal and energy homeostatic systems is still poorly understood (*18*, *41*–*43*). The BAT represents a common crucial target of the two homeostatic systems, which is a major organ for non-shivering adaptive thermogenesis and contributes to total EE in mice [up to 60%; (*44*)] and humans (*45*). We reveal that warm-activated LPB$^{Pdyn}$ neurons inhibit BAT thermogenesis to reduce $T_{core}$ and EE (Fig. 5, B and J, and fig. S3). This induced hypothermia by activating LPB$^{Pdyn}$ neurons still exists at the thermal neutral temperature (fig. S4C), suggesting that the BAT thermogenesis is not entirely off at this temperature and could still be inhibited to lower $T_{core}$. Consistently, previous recordings of BAT sympathetic nerve activity reveal a gradual inhibition by skin warming (*12*). Furthermore, the rise of $T_{iBAT}$ lags behind the rise of $T_{core}$ during environmental warming (Fig. 1, F to H). Thus, these data lead us to propose that BAT thermogenesis is gradually inhibited by warm temperature rather than being completely shut off by $T_a$ higher than the low critical temperature suggested before (*46*). Above the low critical temperature, BAT thermogenesis may still contribute to the basal EE, which awaits further studies.

Manifestly, blocking $LPB^{Pdyn}$ neurons elevates $T_{iBAT}$ and EE and is sufficient to limit body weight gain driven by HFD (Fig. 7E and fig. S9). Also, $LPB^{Pdyn}$ neural function is sensitive to fasting, which is consistent with the fact that fasting suppresses BAT thermogenesis (*47*). Therefore, our molecular identification of a selective negative regulator of BAT thermogenesis may present a genetic entry to investigate the fundamental interconnections between homeostatic systems, which might be helpful for the anti-obesity endeavor.

### Thermoregulatory neurons to cold temperature in the LPB and the POA

The LPBd and LPBel are important for thermoregulation in response to warm and cold temperatures, respectively (*12*, *13*, *25*). Understandably, broad optogenetic activation of LPB glutamatergic soma can induce hypothermia or hyperthermia (fig. S1D). However, the LPB in mice is rather small, which prevents subarea-specific functional modulations from separating warm- and cold-induced thermoregulatory neurons. Instead, we sought for genetic and projection-specific approaches to define thermoregulatory neurons to warm temperatures. It is still unclear about the genetic identity of LPB thermoregulatory neurons to cold temperatures.

Similarly, it is evident that the POA is a thermoregulation center for both warm and cold temperatures (*5*, *6*). Unexpectedly, most recent reports only support the existence of warm-induced thermoregulatory neurons, as their activation only induced hypothermia (*14*–*16*, *18*–*20*). By using genetically encoded neurotoxin TeNT, we blocked POA glutamatergic neurons and found that they are required for both cold- and warm-induced thermoregulation (fig. S6). Therefore, more specific molecular interrogations are required to reveal mechanisms for cold-induced thermoregulation.

### Role of Pdyn signaling in thermoregulation

The Pdyn protein is enzymatically cleaved to produce Dynorphins (Dyn), which are endogenous opioids for kappa opioid receptors (KORs). The Dyn/KOR signaling has been suggested to regulate body temperatures for decades (*48*–*50*). Activation of $Pdyn^{+}$ neurons in the LPB and the arcuate nucleus induce hypothermia (*33*). We show that $LPB^{Pdyn}$ neurons release glutamate to excite POA neurons to induce hypothermia. Consistently, low-frequency photostimulation (5 Hz), which may not be high enough to trigger the release of neuropeptides, still induces hypothermia (fig. S4B). Thus, our finding suggests the $LPB^{Pdyn}$ circuitry controls body temperature via releasing glutamate. Nevertheless, how dynorphins are released and whether it acts on POA neurons to regulate body temperature remain to be tested.

### Downstream heat defense pathways

As illustrated in Fig. 8I, we suggest that the bifurcation of BAT thermogenesis and vasodilation occurs as early as the LPB. Then, POA glutamatergic neurons are the targets for LPB neurons based on transsynaptic labeling (fig. S1I) and POA glutamatergic neural blocking [Fig. 5L; (*12*)]. VMPO LepR neurons are not required for the hypothermic effect of $LPB^{Pdyn}$ neurons (fig. S7C). $VMPO^{BDNF/PACAP}$ neurons might (in part) be the targets as they can inhibit iBAT thermogenesis and activate tail vasodilation (*16*, *19*). More specific genetic manipulations are needed to separate the two functions, as well as the shivering control function in the POA. Next, the vasodilation neurons in the POA may directly target neurons in the raphe pallidus nucleus (RPa) to regulate vasomotor responses (*51*). The DMH might not be needed for vasodilation, as activation of glutamatergic neurons there does not induce tail vasodilation (*52*). Neurons for inhibiting shivering and BAT thermogenesis appear to share a similar pathway where POA glutamatergic neurons may first activate POA GABAergic neurons such as these in the vLPO (*16*, *23*). Then, POA GABAergic neurons may directly inhibit RPa neurons to reduce shivering and BAT thermogenesis (*23*, *53*, *54*) or they may indirectly inhibit RPa neurons via inhibiting DMH glutamatergic neurons (*43*, *52*, *55*) (Fig. 8I). Notably, neurons for inhibiting shivering and BAT thermogenesis are separable, as $LPB^{CCK}$ neurons can substantially suppress shivering activity without affecting BAT thermogenesis (Figs. 5 and 6).

### Role of physical activity in thermoregulation

Physical activity fluctuates along with $T_{core}$ and EE in light-dark cycles (fig. S10, A to C), suggesting that it might contribute to thermoregulation. Consistently, heat defense neurons in the POA and the LPB reduce physical activity upon activation [Fig. 5E and 6F; (*16*, *18*)], and broad activation of DMH $Vglut2^{+}$ or $Vgat^{+}$ neurons increase $T_{core}$ along with an increase in physical activity (*16*, *52*). However, careful analysis reveals that physical activity levels are not changed significantly by cold exposure (10° to 15°C) or warm exposure (35°C) [figs. S8, F and G, and S10, G and H; (*16*)]. Accordingly, the EE caused by physical activity stays at a similar level across $T_a$ ranging from 4° to 32°C, and the increased $T_{core}$ during exercise might be due to a higher set point in $T_{core}$, not simply due to heat production during exercise (*44*, *56*). Therefore, physical activity may contribute less to $T_{core}$ changes than expected, which might provide an explanation for the little effect on the basal physical activity seen after blocking $LPB^{Pdyn/CCK}$ neurons (figs. S8C and S10C), and activation of a subset of DMH neurons ($Brs3^{+}$) increased $T_{core}$ without affecting physical activity (*43*). It is still unclear why activation of $LPB^{Pdyn/CCK}$ neurons reduced physical activity only after photostimulation (Fig. 5E and 6F), which might be due to an unknown secondary effect caused by hypothermia. Nevertheless, prolonged excise increases $T_{core}$ set point and enhances vasodilation, which then reduces the risk of hyperthermia (*56*, *57*). In conjunction with this, athletes with spinal cord injuries may have a higher risk of hyperthermia due to variations in the set points and impaired sympathetic control of vasodilation and sweating below the injury level (*58*). Therefore, it is interesting to check how exercise imposes an effect on central thermoregulatory neurons such as those in the LPB and POA to affect thermoregulation.

## MATERIALS AND METHODS

### Experimental animals

Animal care and use conformed to institutional guidelines of ShanghaiTech University, Shanghai Biomodel Organism Co., and governmental regulations. All experiments were performed on male adult mice (8 to 16 weeks old; for TeNT mice, may last to 25 weeks). Mice were housed under controlled temperature (22° to 25°C) in a 12-hour reverse light/dark cycle (light time, 8 p.m. to 8 a.m.) with ad libitum chow food (4% fat specific pathogen–free rodent feed; SLAC, no. M03) and water. Pdyn-IRES-Cre mice (JAX, no. 027958), CCK-IRES-Cre mice (JAX, no. 012706), Vgat-IRES-Cre mice (JAX, no. 028862), Vglut2-IRES-Cre mice (JAX, no. 028863), and Ai14 mice (JAX, no. 007914) were purchased from the Jackson laboratory. Gal-Cre mice (031060-UCD) and C57BL/6J mice (JAX, no. 000664)

were purchased from MMCCR (Mutant Mouse Regional Resource Center) and Silaike Experiment Animal Co. Ltd. (Shanghai), respectively. The EEF1A1–LSL.EGFPL10 mice were gifted by J. Friedman. The Gad67-GFP mice were gifted by N. Tamamaki. The Rosa26-FSF-tdTomato mice were gifted by J. Huang. Vglut2-T2A-Flpo mice were made through the CRISPR-Cas9 gene targeting by the core facility of Peking Union Medicine College. Briefly, *Mus musculus* C57BL/6J-Vglut2-T2A-Flpo was generated by inserting a T2A-NLS-Flpo sequence right before the stop codon through CRISPR-Cas9 gene editing. The T2A-NLS-Flpo sequence is:

gagggcagaggaagtcttctaacatgcggtgacgtggaggagaatcccggcccttccatggctcctaagaagaagaggaaggtgatgagccagttcgacatcctgtgcaagaccccccccaaggtgctggtgcggcagttcgtggagagattcgagaggcccagcggcgagaagatcgccagctgtgccgccgagctgacctacctgtgctggatgatcacccacaacggcaccgccatcaagagggccaccttcatgagctacaacaccatcatcagcaacagcctgagcttcgacatcgtgaacaagagcctgcagttcaagtacaagacccagaaggccaccatcctggaggccagcctgaagaagctgatccccgcctgggagttcaccatcatcccttacaacggccagaagcaccagagcgacatcaccgacatcgtgtccagcctgcagctgcagttcgagagcagcgaggaggccgacaagggcaacagccacagcaagaagatgctgaaggccctgctgtccgaggcgagagcatctgggagatcaccgagaagatcctgaacagcttcgagtacaccagcaggttcaccaagaccaagaccctgtaccagttcctgttcctggccacattcatcaactgcggcaggttcagcgacatcaagaacgtggaccccaagagcttcaagctggtgcagaacaagtacctggcgtgatcattcagtgcctggtgaccgagaccaagacaagcgtgtccaggcacatctactttttcagcgccagaggcaggatcgacccccctggtgtacctggacgagttcctgaggaacagcgagcccgtgctgaagagagtgaacaggaccggcaacagcagcagcaacaagcaggagtaccagctgctgaaggacaacctggtgcgcagctacaacaaggccctgaagaagaacgccccctaccccatcttcgctatcaagaacggccctaagagccacatcggcaggcacctgatgaccagctttctgagcatgaagggcctgaccgagctgacaaacgtggtgggcaactggagcgacaagagggcctccgccgtggccaggaccacctacacccaccagatcaccgccatccccgaccactacttcgccctggtgtccaggtactacgcctacgaccccatcagcaaggagatgatcgccctgaaggacgagaccaaccccatcgaggagtggcagcacatcgagcagctgaagggcagcgccgagggcagcatcagatacccgcctggaacggcatcatcagccaggaggtgctggactacctgagcagctacatcaacaggcggatctga. note = humanized flippase (85-1356), note = NLS (64-84), /note = "T2A"(1..54). Target site 1 (5′- GGTAGCACCGTAAGATTTGGTGG-3′) located on Vglut2 coding exon and target site 2 (5′-GGTTTCCTGTAGAAATAAGTAGG-3′) located on its 3′ untranslated region (3′UTR) were selected for the integration of the T2A-NLS-Flpo sequence right before the stop codon (TAA). Their corresponding guide sequences are M-Vglut2-E2A-g-up (5′- TAGGTAGCACCGTAAGATTTGG-3′), M-Vglut2-E2A2-g-down (5′-AACCCAAATCTTACGGTGCTA-3′) or M-Vglut2-E2B-g-up (5′- TAGGTTTCCTGTAGAAATAAGT-3′), and M-Vglut2-E2B-g-down (5′- AAACACTTATTTCTACAGGAAA-3′) were annealed and inserted into the entry site of pX330 and named pX330-Vglut2-EA and pX330-Vglut2-EB, respectively. Together with a donor plasmid, pVglut2/T2A-Flpo contained two arms of Vglut2 gDNAs and a T2A-Flpo sequence. The 5′-arm is an 1111–base pair (bp) sequence before the Vglut2 stop codon, and 3′-arm is an 1175-bp sequence after the Vglut2 stop codon. A T2A-Flpo coding sequence was inserted between the two arms. To avoid targeting by the sgRNAs, the corresponding sites on the donor were mutated without changing amino acid sequence [CC(A)ACCAAATCT(C)TACGGTGCTACC and GGTTTCCTGTAGAAATAAGTAGG(C)]. The pVglut2/T2A-Flpo, pX330-Vglut2-EA, and pX330-Vglut2-EB were injected into fertilized oocytes, and survived embryos were transferred to pseudopregnant females. Mice produced were genotyped by genomic DNA purified from the tail and amplified with LA Taq HS DNA polymerase (Takara, RR042) with the upstream primer (5′-AGAATGGAGGCTGGCCTAAC-3′) and the downstream primer (mu-R: 5′-atgtcgaagctcaggctgtt-3′ and wt-R: 5′ CAAGACTTGCTTGGTTGATATGTT-3′) to produce a 397-bp product for the modified allele and a 217-bp production for the wild-type allele.

### Stereotaxic brain injection

We delivered ~0.15 μl (unless specified) of AAV through a pulled glass pipette and a pressure microinjector (Nanoject II, no. 3-000-205A, Drummond) at a slow rate (23 nl $min^{-1}$) with customized controllers. The injection needle was withdrawn 10 min after the end of the injection, and the injection coordinates were calculated according to Paxinos and Franklin mice brain coordinates (third edition), and the injection was performed using a small animal stereotaxic instrument (David Kopf Instruments, no. PF-3983; RWD Life Science, no. 68030; Thinker Tech Nanjing Biotech, no. SH01A) under general anesthesia by isoflurane. A feedback heater was used to keep mice warm during surgeries. Mice were recovered in a warm bracket before they were transferred to housing cages for 2 to 4 weeks before performing behavioral evaluations. The fiber optic cables (200 μm in diameter; Inper Inc., China) were chronically implanted and secured with dental cement (C&B Metabond Quick Adhesive Cement System, Parkell, Japan).

Stereotaxic coordinates are as follows: LPB, AP: −4.95 mm, ML: ±1.5 mm, DV: −3.60 mm ~ −3.75 mm (mouse strain Pdyn-Cre); LPB, AP: −5.3 mm, ML: ±1.5 mm, DV: −3.6 mm ~ −3.7 mm (mouse strain CCK-Cre); VMPO, AP: 0.75 mm, ML: 0 mm, DV: −4.5 mm ~ −5.0 mm (vLPO); AP: 0.35 mm, ML: ±0.75 mm, DV: −5.3 mm (DMD); AP: −1.25 mm, ML: ±0.3 mm, DV: −5.0 mm (DMD); and AP: −1.25 mm, ML: ±1.0 mm, DV: −4.8 mm, angle: 8°(L/R)

AAVs are as follows: AAV2-Retro-hEF1a-FLEX-GFPL10-WPRE-hGHpA, AAV2/8-hEF1a-FLEX-GFPL10-WPRE-hGHpA, AAV2/9-hSyn-Flex-GCaMP6s-WPRE-SV40pA, AAV2/9-hSyn-DIO-jGCaMP7b-WPRE-pA, AAV2/9-hSyn-DIO-Synapse-jGCaMP7b-WPRE-pA, AAV2/9-CAG-Flex-rev-oChIEF-tdTomato, AAV2/8-CAG-Flex-rev-oChIEF-tdTomato, AAV2/9-hSyn-DIO-hM3D(Gq)-EGFP (enhanced GFP), AAV2/8-hSyn-DIO-hM3D(Gq)-mCherry, AAV2/9-EF1a-DIO-EGFP-WPRE-pA, AAV2/9-EF1a-DIO-mRuby-WPRE-pA, AAV2/9-hEF1a-fDIO-mCherry-2A-TetTox-WPRE-pA, AAV2/9-hEF1a-DIO-mCherry-2A-TetTox-WPRE-pA, AAV2/9-CMV-bGlobin-DIO-GFP-2A-TetTox, AAV2/1-CMV-bGlobin-Cre-EGFP, AAV2/9-hSyn-FLEX-mGFP, and AAV2/9-hSyn-FLEX-Tdtomato (all were purchased from Shanghai Taitool Bioscience Co.).

### Immunohistochemistry

Mice were anesthetized with isoflurane and perfused transcardially with phosphate-buffered saline (PBS) followed by 4% paraformaldehyde (PFA) in PBS. Brain tissues were postfixed overnight at 4°C and then sectioned at 50-μm thicknesses using a vibratome (Leica, VT1200S). For glutamate staining, mice were perfused transcardially with PBS followed by 50-ml 4% PFA in PBS without postfixation (*59*). Brains were isolated and immersed in 20% sucrose for 1 day and 30% sucrose for 2 days at 4°C before being sectioned at 40-μm thicknesses on a cryostat microtome (Leica, CM3050s). Brain slices were collected and blocked with blocking solution containing 2% (v/v) normal goat serum, 2.5% (w/v) bovine serum albumin, 0.1% (v/v) Triton X-100, and 0.1% (w/v) $NaN_3$ in PBS for 2 hours at room temperature and subsequently incubated with primary antibodies for 2 days at 4°C. Then, the samples followed by washing three times in PBST [PBS with 0.1% (v/v) Triton X-100] before incubation in secondary antibodies for overnight at 4°C. For glutamate

staining, brain slices were collected and blocked with a blocking solution containing 10% (v/v) normal goat serum and 0.1% (v/v) Triton X-100 in PBS for overnight at 4°C and subsequently incubated with primary antibodies for 8 hours at room temperature. After that, the slices were washed three times in PBST [PBS with 0.7% (v/v) Triton X-100) before incubation in secondary antibodies for 2 hours at room temperature. Primary antibodies include chicken anti-GFP (1:1000; Abcam, no. ab13970), rabbit anti–neuropeptide S (1:500; Abcam, no. ab18252), rabbit anti-cfos (1:10,000; Synaptic Systems, no. 226003), guinea pig anti-cfos (1:500; Synaptic Systems, no. 226004), rat anti–red fluorescent protein (1:1000; Chromotek, no. 5F8), rabbit anti-glutamate [1: 1000; Sigma-Aldrich, no. G6642-.2ML; see (*59*) for validation], rabbit anti–Dynorphin A (1:500; Phoenix Pharmaceuticals, no. H-021-03), and guinea pig anti-prodynorphin (1:500; GeneTex, GTX10280). Secondary antibodies include DyLight 488–conjugated goat anti-chicken immunoglobulin G (IgG) (1:1000; Invitrogen, no. SA5-10070), Alexa Fluor 594–conjugated goat anti-rat IgG (1:1000; Invitrogen, no. A-11007), Alexa Fluor 594–conjugated goat anti-rabbit IgG (1:1000; Jackson ImmunoResearch Laboratories, no. 111-585-144), Alexa Fluor 594–conjugated goat anti–guinea pig IgG (1:1000; Invitrogen, no. A-11076), and Alexa Fluor 647–conjugated goat anti-rabbit IgG (1:1000; Invitrogen, no. A21244). Brain sections were then washed three times in PBST and coverslipped with 4′,6-diamidino-2-phenylindole Fluoromount-G mounting medium (SouthernBiotech, no. 0100-20). Images were captured on a Nikon A1R or Leica SP8 confocal microscope or Olympus VS120 Virtual Microscopy Slide Scanning System.

To stain Pdyn and Dynorphin A, mice were treated with 40 μg of colchicine (Sigma-Aldrich, C9754) in 1 μl of $H_2O$ through intracerebraventricular injection with a pulled glass pipette and a pressure microinjector (Nanoject II, no. 3-000-205A, Drummond) at a slow rate (46 nl $min^{-1}$) with customized controllers. Coordinates were 1.0 mm lateral, 0.4 mm back from the bregma, and 2.5 mm below the skull. Injection began 5 min after tissue penetration, and pulled glass pipette was pulled out 10 min after injection. After suturing, mice were recovered in a warm bracket before they were transferred to housing cages for 72 hours before perfusion.

### Cell type–specific retro-TRAP and sequencing

A recombinant Cre-dependent AAV plasmid expressing GFP-tagged ribosomal subunit L10a (AAV2-EF1a-DIO-EGFP-L10a) was gifted by J. Friedman and then packaged using rAAV2-retro capsids by Taitool. Three hundred nanoliters of the viral aliquot was injected into the VMPO of Vglut2-IRES-Cre mice. Animals were euthanized for immunoprecipitation 4 weeks after injection.

For TRAP experiments, brain slices containing the LPB regions were prepared from virus-injected mice anesthetized with isoflurane before decapitation. Brains were removed and placed in ice-cold diethyl pyrocarbonate–PBS. Coronal brain slices (300 μm) were cut using a vibratome (VT1200S, Leica Microsystems, Germany). The slices were incubated at ice-cold dissection buffer in a 60-mm dish and placed under a stereomicroscope. Then, the two LPB regions of each slice were cut out with microsurgical forceps with a 150-μm width tip. Tissue from six brains was pooled for each experimental repeat, and a total of three experimental repeats were performed. Pooled tissue was homogenized and clarified by centrifugation. Ribosomes were immunoprecipitated using anti-EGFP antibodies (an equal mixture of clones 19C8 and 19F7 from Monoclonal Antibody Core Facility at Memorial Sloan-Kettering Cancer Center) that were previously conjugated to Protein L–coated magnetic beads (Thermo Fisher Scientific) for 16 hours in 4°C with rotating. An aliquot of input RNA was taken before immunoprecipitation, and total immunoprecipitated RNA was then purified using the RNAeasy Micro kit (QIAGEN). The products were then purified and enriched with polymerase chain reaction (PCR) to create the final complementary DNA library. Purified libraries were quantified by Qubit 2.0 Fluorometer (Life Technologies, USA) and validated by Agilent 2100 Bioanalyzer (Agilent Technologies, USA) to confirm the insert size and calculate the mole concentration. The cluster was generated by cBot with the library diluted to 10 pM and then was sequenced on the Illumina NovaSeq 6000 (Illumina, USA). The library construction and sequencing were performed by Shanghai Sinotech Genomics Corporation (China).

### TRAP-seq data analysis

The RNA quantification data after sequencing were analyzed as the following. First, the RNA in the IP for each gene was divided by the input to determine the statistical significance and fold enrichment (IP/Input). The hits were narrowed down by only analyzing the PB-enriched gene list downloaded from Allen Institute (https://alleninstitute.org/; tool one: MOUSE BRAIN CONNECTIVITY-source search-filter source structure: Parabrachial nucleus; tool two: MOUSE BRAIN-Fine Structure Search: Parabrachial nucleus). The top candidate genes were then selected for further quantitative PCR analysis.

### Metabolic measurement

For DREADDs and TeNT mice, EE, locomotor activity, food intake, and body temperature were monitored by Comprehensive Lab Animal Monitoring System with Temperature Telemetry Transmitter (CLAMS; Columbus Instruments, with G2 E-Mitter transponders). The data were acquired at a 10-min interval per data point as shown in the figures. Temperature transponders were implanted into the peritoneal cavity 3 to 5 days before testing. Stimuli (drugs or temperature) were delivered between 10 a.m. and 3 p.m. (for long-time stimuli, it may occur between 2 p.m. to 8 p.m.) in the dark phase. Mice were adapted in the metabolic chambers for 2 days before giving saline [volume (μl) = 10 × body weight (grams)], CNO (0.1 to 2.5 mg/kg body weight, i.p.; ENZO, no. BML-NS105-0025, as indicated in each figure), CL316243 (1 mg/kg body weight, i.p.; Merck, no. 5.04761.0001), IL-1β (3 μg/kg body weight, i.p.; Sigma-Aldrich, no. SRP8033).

### Tail, iBAT, and core body temperature measurement

For C57BL/6J and TeNT (as to their controls) injected mice, tail temperatures and BAT temperatures were measured using a thermal infrared camera (A655sc, FLIR). Snapshot images were taken at the specified time points, and an average of three spot readings was taken at the middle of the tail and interscapular region, which was shaved 3 to 5 days before measurement. For optogenetic mice, the BAT temperature was measured three times for average using subcutaneous implanted thermal probes (IPTT-300, Biomedic Data Systems, DE) inserted at the midline in the interscapular region under anesthesia at least 1 week before the start of the experiment. Measurements were taken with the noncontact DAS-7007 reader. Core temperature and physical activity of optogenetic mice were recorded at a 1-min interval by VitalView Data Acquisition System Series 4000 (Mini-Mitter, Oregon, USA) with G2 E-Mitter transponders. All measurements were conducted during the dark phase.

For wired recording, we used a modified thermocouple temperature measuring device. Two T-type thermocouples (TT-40) were

implanted in the abdomen and interscapular region of the mice, respectively, to measure core body temperatures and BAT temperatures. Before implantation, we tested the linear temperature change to make sure that the measurement was accurate. The implantation was done 3 to 5 days before measurement. National Instrument (NI) data acquisition card (USB-TC01) and supporting software were used for data collection. The sampling rate was 1 Hz.

### iBAT sympathetic nerve denervation

Mice were anesthetized with isoflurane. The hair in the targeted area was shaved, and the area was wiped with 95% ethanol-soaked sterile gauze. A midline incision was made in the skin along the upper dorsal surface to expose both iBAT pads followed by additional application of styptic powder to the area to prevent bleeding. We gently exposed the medial, ventral surface of both pads to visualize nerves beneath the pad. Nerves were checked under a microscope. All five nerves of both pads were cut off a length of 2 to 3 mm to avoid nerve regeneration. Mice were housed at the thermoneutral environment for 5 to 7 days for recovery before measurements.

### EMG recording

Mice were anesthetized with isoflurane and fixed with the animal stereotaxic instrument to avoid movement. The mouse abdomen was put on an aluminum thermal pad whose temperature was controlled by circulating water to maintain body temperature at 36° ± 1.5°C. Rectal temperature was monitored with a thermocouple as an indication of body core temperature. Another thermocouple to monitor skin temperature was taped onto the abdominal skin, which was put on the thermal pad. Handmade electrodes for EMG recording were inserted into nuchal muscles, and the signal was filtered (10 to 1000 Hz) and amplified (×1000) with a Model 1800 2-Channel Microelectrode AC Amplifier (A-M Systems, Sequim, WA, USA). To induce shivering, the circulating water was switched to ice-cold water, and each cooling episode lasted about 10 min until the laser stimulations were done. The EMG amplitude was quantified (Spike 2, CED, Cambridge, UK) in sequential 4-s bins as the square root of the total power (root mean square) in the 0 to 500 Hz band of the autospectra of each 4-s segment of EMG as shown in (*60*). Temperatures were recorded by NI data acquisition card (USB-TC01) and supporting software.

### Temperature preference test

Mice were separated into individual cages for at least 7 days. A custom two-chamber cage was placed on temperature-controlled plates, adjusted such that one end of the cage was at 32° ± 0.5°C, while the other end of the cage was at 20° or 35° ± 0.5°C. Mice were allowed to explore the chamber for 30-min per day for 3 days. During this habituation period, both of the two plates were adjusted to 32° ± 0.5°C. On the fourth day, the plates were adjusted to either 32° ± 0.5°C or 20° (35°) ± 0.5°C. During this testing phase, individual mice were put into either chamber and allowed to freely explore all chambers for 30 min. For each trial, the orientation of the plate and cage was randomized. The position of the mouse was recorded using Digbehv video-recording software (Jiliang, Shanghai, China). All tests were performed from 10 a.m. to 5 p.m. in the dark phase.

### Food intake assay and blood glucose measurement

For the food intake shown in figs. S3 (K and S) and S9K, the food intake assays were performed in the home cage. Mice were separated for at least 5 days and then fasted for 24 hours from 10 a.m. to 10 a.m. before the assay. DREADD injected mice were injected with saline or CNO, and measurement of food intake was made at 1, 2, 3, and 4 hours after injection. CNO injections were at a concentration of 2.5 mg/kg body weight. For the food intake shown in figs. S3 (J and R) and S9E, food intake was monitored by the CLAMS with free access to food. Blood glucose concentrations were measured from the tail vein using a hand-held glucometer (Accu-Chek Performa Connect, Roche, Switzerland). CNO injections were at a concentration of 2.5 mg/kg body weight.

### Slice physiological recording

Brain slices recording and data analysis were performed similarly as described in (*61*). Briefly, slices containing the VMPO regions were prepared from adult mice anesthetized with isoflurane before decapitation. Brains were removed and placed in ice-cold–oxygenated (95% $O_2$ and 5% $CO_2$) cutting solution (228 mM sucrose, 11 mM glucose, 26 mM $NaHCO_3$, 1 mM $NaH_2PO_4$, 2.5 mM KCl, 7 mM $MgSO_4$, and 0.5 mM $CaCl_2$). Coronal brain slices (250 μm) were cut using a vibratome (VT1200S, Leica Microsystems, Germany). The slices were incubated at 32°C in oxygenated artificial cerebrospinal fluid (ACSF; 119 mM NaCl, 2.5 mM KCl, 1 mM $NaH_2PO_4$, 1.3 mM $MgSO_4$, 26 mM $NaHCO_3$, 10 mM glucose, and 2.5 mM $CaCl_2$) for 1 hour and were then kept at room temperature under the same conditions before transfer to the recording chamber. The ACSF was perfused at 2 ml/min. The acute brain slices were visualized with a 40× Olympus water immersion lens, differential interference contrast optics (Olympus Inc., Japan), and a charge-coupled device camera (IR1000, Dage-MTI, USA).

Patch pipettes were pulled from borosilicate glass capillary tubes (no. BF150-150-86-10, Sutter Instruments, USA) using a P-97 pipette puller (Sutter Instruments, USA). For EPSC recordings, pipettes were filled with solution (135 mM potassium gluconate, 4 mM KCl, 10 mM Hepes, 4 mM Mg–adenosine 5′-triphosphate, 0.3 mM $Na_3$-guanosine 5′-triphosphate, and 10 mM sodium phosphocreatine) (pH 7.2, 275 mOsm). For EPSC recordings, cells were clamped at −70 mV; to block EPSCs, 10 μM CNQX (Sigma-Aldrich) and 50 μM DL-AP5 (Tocris) were applied to the bath solution. The resistance of pipettes varied between 3 and 5 megohm. The signals were recorded with MultiClamp 700B, Digidata 1440A interface, and Clampex 10 data acquisition software (Molecular Devices). After the establishment of the whole-cell configuration, series resistance was measured. Recordings with series resistance >20 megohm were rejected. Blue light pulses were delivered through the 40× objective of the microscope, with the X-Cite light-emitting diode light source. Light power density was adjusted to 7 $mW/mm^2$.

### Calcium fiber photometry

Following injection of an AAV2/9-hSyn-Flex-GCaMP6s or AAV2/9-hSyn-DIO-jGCaMP7b-WPRE-pA viral vector, an optical fiber (200 μm O.D. (outer diameter), 0.37 numerical aperture; Inper Inc., China) was placed 150 μm above the viral injection site. Postsurgery mice were allowed to recover for at least 2 weeks before any studies were performed. Fluorescence signals were acquired with a dual-channel fiber photometry system (Fscope, Biolinkoptics, China) equipped with a 488-nm excitation laser (OBIS, Coherent), 505- to 544-nm emission filter, and a photomultiplier tube (PMT) (Hamamatsu, no. R3896). The gain (voltage) on PMT was set to 600 V. The laser power at the tip of the optical fiber was adjusted to as low as possible (~25 μW) to minimize bleaching. The analog voltage signals fluorescent were low pass (30 Hz) filtered and digitalized at 100 Hz, which were then

recorded by Fscope software (Biolinkoptics, China). Mice behaviors were recorded by a top-view positioned camera (Logitech, no. C930e). We used a screen recorder (EV Capture, Hunan Yiwei LTD, China) to synchronize behavioral videos and analog voltage signals of fluorescence.

All animals were allowed to recover after fiber cord attachment for at least 30 min. For temperature challenges, the custom-build Peltier floor plate (15 cm by 15 cm) temperature for each individual mouse was controlled by a Peltier controller (no. 5R7-001, Oven Industry) with customized LabVIEW code (NI), and mouse was caged in an acrylic chamber (15 cm by 15 cm by 30 cm), which placed on the plate. For tested stimuli presentation, the following items were sequentially placed into the cage for 30-min each: novel object (plastic ball and aluminum block), normal chow, HFD (Research Diets, no. D12492), and novel mouse of the same sex.

### Fiber photometry data analysis

The data analysis has been previously described (*16*, *59*). Basically, to calculate the fluorescence change ratios, the raw data were analyzed using Fscope software and customized MATLAB code. We segmented the data based on behavioral events within individual trials. We derived the values of fluorescence change ($\Delta F/F_0$) by calculating $(F - F_0)/F_0$, where $F_0$ is the baseline fluorescence signal averaged in a time window before events (temperature changes and introductions of food, novel objects, or mouse as indicated) indicated in the figure legends. Last, we plotted the average of fluorescence changes ($\Delta F/F_0$) with different behavioral events using Customized MATLAB code and GraphPad Prism 8 (GraphPad).

### Code availability

The code that supports the findings of this study is available from the corresponding author upon reasonable request.

## SUPPLEMENTARY MATERIALS

Supplementary material for this article is available at http://advances.sciencemag.org/cgi/content/full/6/36/eabb9414/DC1

View/request a protocol for this paper from *Bio-protocol*.

## REFERENCES AND NOTES


1. T. P. Yeo, Heat stroke: A comprehensive review. *AACN Clin. Issues* **15**, 280–293 (2004).
2. E. W. Freeman, K. Sherif, Prevalence of hot flushes and night sweats around the world: A systematic review. *Climacteric* **10**, 197–214 (2007).
3. F. G. Gaudio, C. K. Grissom, Cooling methods in heat stroke. *J. Emerg. Med.* **50**, 607–616 (2016).
4. L. L. Sievert, Subjective and objective measures of hot flashes. *Am. J. Hum. Biol.* **25**, 573–580 (2013).
5. C. L. Tan, Z. A. Knight, Regulation of body temperature by the nervous system. *Neuron* **98**, 31–48 (2018).
6. S. F. Morrison, K. Nakamura, Central neural pathways for thermoregulation. *Front. Biosci.* **16**, 74–104 (2011).
7. K. Nakamura, Central circuitries for body temperature regulation and fever. *Am. J. Physiol. Regul. Intergr. Comp. Physiol.* **301**, R1207–R1228 (2011).
8. E. S. Bachman, H. Dhillon, C.-Y. Zhang, S. Cinti, A. C. Bianco, B. K. Kobilka, B. B. Lowell, βAR signaling required for diet-induced thermogenesis and obesity resistance. *Science* **297**, 843–845 (2002).
9. F. Wang, E. Bélanger, S. L. Côté, P. Desrosiers, S. A. Prescott, D. C. Côté, Y. De Koninck, Sensory afferents use different coding strategies for heat and cold. *Cell Rep.* **23**, 2001–2013 (2018).
10. C. Ran, M. A. Hoon, X. Chen, The coding of cutaneous temperature in the spinal cord. *Nat. Neurosci.* **19**, 1201–1209 (2016).
11. Y. Xue, Y. Yang, Y. Tang, M. Ye, J. Xu, Y. Zeng, J. Zhang, In vitro thermosensitivity of rat lateral parabrachial neurons. *Neurosci. Lett.* **619**, 15–20 (2016).
12. K. Nakamura, S. F. Morrison, A thermosensory pathway mediating heat-defense responses. *Proc. Natl. Acad. Sci. U.S.A.* **107**, 8848–8853 (2010).
13. K. Nakamura, S. F. Morrison, A thermosensory pathway that controls body temperature. *Nat. Neurosci.* **11**, 62–71 (2008).
14. D. Kroeger, G. Absi, C. Gagliardi, S. S. Bandaru, J. C. Madara, L. L. Ferrari, E. Arrigoni, H. Münzberg, T. E. Scammell, C. B. Saper, R. Vetrivelan, Galanin neurons in the ventrolateral preoptic area promote sleep and heat loss in mice. *Nat. Commun.* **9**, 4129 (2018).
15. E. C. Harding, X. Yu, A. Miao, N. Andrews, Y. Ma, Z. Ye, L. Lignos, G. Miracca, W. Ba, R. Yustos, A. L. Vyssotski, W. Wisden, N. P. Franks, A neuronal hub binding sleep initiation and body cooling in response to a warm external stimulus. *Curr. Biol.* **28**, 2263–2273.e4 (2018).
16. Z.-D. Zhao, W. Z. Yang, C. Gao, X. Fu, W. Zhang, Q. Zhou, W. Chen, X. Ni, J.-K. Lin, J. Yang, X.-H. Xu, W. L. Shen, A hypothalamic circuit that controls body temperature. *Proc. Natl. Acad. Sci. U.S.A.* **114**, 2042–2047 (2017).
17. S. B. G. Abbott, C. B. Saper, Median preoptic glutamatergic neurons promote thermoregulatory heat loss and water consumption in mice. *J. Physiol.* **595**, 6569–6583 (2017).
18. S. Yu, E. Qualls-Creekmore, K. Rezai-Zadeh, Y. Jiang, H.-R. Berthoud, C. D. Morrison, A. V. Derbenev, A. Zsombok, H. Münzberg, Glutamatergic preoptic area neurons that express leptin receptors drive temperature-dependent body weight homeostasis. *J. Neurosci.* **36**, 5034–5046 (2016).
19. C. L. Tan, E. K. Cooke, D. E. Leib, Y.-C. Lin, G. E. Daly, C. A. Zimmerman, Z. A. Knight, Warm-sensitive neurons that control body temperature. *Cell* **167**, 47–59.e15 (2016).
20. H. W. Kun Song, G. B. Kamm, J. Pohle, F. de Castro Reis, P. Heppenstall, H. Wende, J. Siemens, The TRPM2 channel is a hypothalamic heat sensor that limits fever and can drive hypothermia. *Science* **353**, 1393–1398 (2016).
21. S. L. Padilla, C. W. Johnson, F. D. Barker, M. A. Patterson, R. D. Palmiter, A neural circuit underlying the generation of hot flushes. *Cell Rep.* **24**, 271–277 (2018).
22. T. A. Wang, C. F. Teo, M. Åkerblom, C. Chen, M. T.-L. Fontaine, V. J. Greiner, A. Diaz, M. T. McManus, Y. N. Jan, L. Y. Jan, Thermoregulation via temperature-dependent $PGD_2$ production in mouse preoptic area. *Neuron* **103**, 309–322.e7 (2019).
23. E. P. S. Conceição, C. J. Madden, S. F. Morrison, Neurons in the rat ventral lateral preoptic area are essential for the warm-evoked inhibition of brown adipose tissue and shivering thermogenesis. *Acta Physiol (Oxf.)* **225**, e13213 (2019).
24. J. C. Geerling, M. Kim, C. E. Mahoney, S. B. G. Abbott, L. J. Agostinelli, A. S. Garfield, M. J. Krashes, B. B. Lowell, T. E. Scammell, Genetic identity of thermosensory relay neurons in the lateral parabrachial nucleus. *Am. J. Physiol. Regul. Integr. Comp. Physiol.* **310**, R41–R54 (2016).
25. A. Kobayashi, T. Osaka, Involvement of the parabrachial nucleus in thermogenesis induced by environmental cooling in the rat. *Pflugers Arch.* **446**, 760–765 (2003).
26. C. Gauriau, J.-F. Bernard, Pain pathways and parabrachial circuits in the rat. *Exp. Physiol.* **87**, 251–258 (2001).
27. D. Mu, J. Deng, K.-F. Liu, Z.-Y. Wu, Y.-F. Shi, W.-M. Guo, Q.-Q. Mao, X.-J. Liu, H. Li, Y.-G. Sun, A central neural circuit for itch sensation. *Science* **357**, 695–699 (2017).
28. M. E. Carter, M. E. Soden, L. S. Zweifel, R. D. Palmiter, Genetic identification of a neural circuit that suppresses appetite. *Nature* **503**, 111–114 (2013).
29. D.-Y. Kim, G. Heo, M. Kim, H. Kim, J. A. Jin, H.-K. Kim, S. Jung, M. An, B. H. Ahn, J. H. Park, H.-E. Park, M. Lee, J. W. Lee, G. J. Schwartz, S.-Y. Kim, A neural circuit mechanism for mechanosensory feedback control of ingestion. *Nature* **580**, 376–380 (2020).
30. A. S. Garfield, B. P. Shah, J. C. Madara, L. K. Burke, C. M. Patterson, J. Flak, R. L. Neve, M. L. Evans, B. B. Lowell, M. G. Myers Jr., L. K. Heisler, A parabrachial-hypothalamic cholecystokinin neurocircuit controls counterregulatory responses to hypoglycemia. *Cell Metab.* **20**, 1030–1037 (2014).
31. J. N. Flak, C. M. Patterson, A. S. Garfield, G. D'Agostino, P. B. Goforth, A. K. Sutton, P. A. Malec, J.-M. T. Wong, M. Germani, J. C. Jones, M. Rajala, L. Satin, C. J. Rhodes, D. P. Olson, R. T. Kennedy, L. K. Heisler, M. G. Myers Jr., Leptin-inhibited PBN neurons enhance responses to hypoglycemia in negative energy balance. *Nat. Neurosci.* **17**, 1744–1750 (2014).
32. T. Luo, S. Yu, S. Cai, Y. Zhang, Y. Jiao, T. Yu, W. Yu, Parabrachial neurons promote behavior and electroencephalographic arousal from general anesthesia. *Front. Mol. Neurosci.* **11**, 420 (2018).
33. R. Cintron-Colon, C. W. Johnson, J. R. Montenegro-Burke, C. Guijas, L. Faulhaber, M. Sanchez-Alavez, C. A. Aguirre, K. Shankar, M. Singh, A. Galmozzi, G. Siuzdak, E. Saez, B. Conti, Activation of kappa opioid receptor regulates the hypothermic response to calorie restriction and limits body weight loss. *Curr. Biol.* **29**, 4291–4299.e4 (2019).
34. A. A. Young, N. J. Dawson, Evidence for on-off control of heat dissipation from the tail of the rat. *Can. J. Physiol. Pharmacol.* **60**, 392–398 (1982).
35. Y.-L. Yang, N. Wang, H.-X. Song, Z.-L. Shen, B. Sun, Y. Tang, Simultaneous telemetric monitoring of the circadian changes in core and BAT temperature in rats: Endogenous vasopressin may contribute to reduced BAT themogenesis and body temperature in the light phase of the circadian cycle. *J. Therm. Biol.* **37**, 316–322 (2012).

36. J. Y. Lin, M. Z. Lin, P. Steinbach, R. Y. Tsien, Characterization of engineered channelrhodopsin variants with improved properties and kinetics. *Biophys. J.* **96**, 1803–1814 (2009).
37. B. Zingg, X.-L. Chou, Z.-G. Zhang, L. Mesik, F. Liang, H. W. Tao, L. I. Zhang, AAV-mediated anterograde transsynaptic tagging: Mapping corticocollicular input-defined neural pathways for defense behaviors. *Neuron* **93**, 33–47 (2017).
38. D. G. R. Tervo, B.-Y. Hwang, S. Viswanathan, T. Gaj, M. Lavzin, K. D. Ritola, S. Lindo, S. Michael, E. Kuleshova, D. Ojala, C.-C. Huang, C. R. Gerfen, J. Schiller, J. T. Dudman, A. W. Hantman, L. L. Looger, D. V. Schaffer, A. Y. Karpova, A designer AAV variant permits efficient retrograde access to projection neurons. *Neuron* **92**, 372–382 (2016).
39. A. R. Nectow, M. V. Moya, M. I. Ekstrand, A. Mousa, K. L. McGuire, C. E. Sferrazza, B. C. Field, G. S. Rabinowitz, K. Sawicka, Y. Liang, J. M. Friedman, N. Heintz, E. F. Schmidt, Rapid molecular profiling of defined cell types using viral TRAP. *Cell Rep.* **19**, 655–667 (2017).
40. P. M. Pilowsky, A. K. Goodchild, Baroreceptor reflex pathways and neurotransmitters: 10 years on. *J. Hypertens.* **20**, 1675–1688 (2002).
41. M. Schneeberger, L. Parolari, T. D. Banerjee, V. Bhave, P. Wang, B. Patel, T. Topilko, Z. Wu, C. H. J. Choi, X. Yu, K. Pellegrino, E. A. Engel, P. Cohen, N. Renier, J. M. Friedman, A. R. Nectow, Regulation of energy expenditure by brainstem GABA neurons. *Cell* **178**, 672–685.e12 (2019).
42. S. Yu, H. Cheng, M. François, E. Qualls-Creekmore, C. Huesing, Y. He, Y. Jiang, H. Gao, Y. Xu, A. Zsombok, A. V. Derbenev, E. A. Nillni, D. H. Burk, C. D. Morrison, H.-R. Berthoud, H. Münzberg, Preoptic leptin signaling modulates energy balance independent of body temperature regulation. *eLife* **7**, e33505 (2018).
43. R. A. Piñol, S. H. Zahler, C. Li, A. Saha, B. K. Tan, V. Škop, O. Gavrilova, C. Xiao, M. J. Krashes, M. L. Reitman, Brs3 neurons in the mouse dorsomedial hypothalamus regulate body temperature, energy expenditure, and heart rate, but not food intake. *Nat. Neurosci.* **21**, 1530–1540 (2018).
44. G. Abreu-Vieira, C. Xiao, O. Gavrilova, M. L. Reitman, Integration of body temperature into the analysis of energy expenditure in the mouse. *Mol. Metab.* **4**, 461–470 (2015).
45. A. Bartelt, J. Heeren, Adipose tissue browning and metabolic health. *Nat. Rev. Endocrinol.* **10**, 24–36 (2014).
46. B. Cannon, J. Nedergaard, Nonshivering thermogenesis and its adequate measurement in metabolic studies. *J. Exp. Biol.* **214**, 242–253 (2011).
47. H.-B. Ruan, M. O. Dietrich, Z.-W. Liu, M. R. Zimmer, M.-D. Li, J. P. Singh, K. Zhang, R. Yin, J. Wu, T. L. Horvath, X. Yang, O-GlcNAc transferase enables AgRP neurons to suppress browning of white fat. *Cell* **159**, 306–317 (2014).
48. M. W. Adler, E. B. Geller, C. E. Rosow, J. Cochin, The opioid system and temperature regulation. *Annu. Rev. Pharmacol. Toxicol.* **28**, 429–449 (1988).
49. M. A. Mittelman-Smith, H. Williams, S. J. Krajewski-Hall, N. T. McMullen, N. E. Rance, Role for kisspeptin/neurokinin B/dynorphin (KNDy) neurons in cutaneous vasodilatation and the estrogen modulation of body temperature. *Proc. Natl. Acad. Sci. U.S.A.* **109**, 19846–19851 (2012).
50. C. da Silveira Scarpellini, L. H. Gargaglioni, L. G. S. Branco, K. C. Bícego, Role of preoptic opioid receptors in the body temperature reduction during hypoxia. *Brain Res.* **1286**, 66–74 (2009).
51. M. Tanaka, M. J. McKinley, R. M. McAllen, Preoptic-raphé connections for thermoregulatory vasomotor control. *J. Neurosci.* **31**, 5078–5088 (2011).
52. N. L. S. Machado, S. B. G. Abbott, J. M. Resch, L. Zhu, E. Arrigoni, B. B. Lowell, P. M. Fuller, M. A. P. Fontes, C. B. Saper, A glutamatergic hypothalamomedullary circuit mediates thermogenesis, but not heat conservation, during stress-induced hyperthermia. *Curr. Biol.* **28**, 2291–2301.e5 (2018).
53. Y. Nakamura, K. Nakamura, S. F. Morrison, Different populations of prostaglandin EP3 receptor-expressing preoptic neurons project to two fever-mediating sympathoexcitatory brain regions. *Neuroscience* **161**, 614–620 (2009).
54. K. Yoshida, X. Li, G. Cano, M. Lazarus, C. B. Saper, Parallel preoptic pathways for thermoregulation. *J. Neurosci.* **29**, 11954–11964 (2009).
55. Y. Zhang, I. A. Kerman, A. Laque, P. Nguyen, M. Faouzi, G. W. Louis, J. C. Jones, C. Rhodes, H. Münzberg, Leptin-receptor-expressing neurons in the dorsomedial hypothalamus and median preoptic area regulate sympathetic brown adipose tissue circuits. *J. Neurosci.* **31**, 1873–1884 (2011).
56. J. S. Haight, W. R. Keatinge, Elevation in set point for body temperature regulation after prolonged exercise. *J. Physiol.* **229**, 77–85 (1973).
57. D. Formenti, N. Ludwig, M. Gargano, M. Gondola, N. Dellerma, A. Caumo, G. Alberti, Thermal imaging of exercise-associated skin temperature changes in trained and untrained female subjects. *Ann. Biomed. Eng.* **41**, 863–871 (2013).
58. M. Attia, P. Engel, Thermoregulatory set point in patients with spinal cord injuries (spinal man). *Paraplegia* **21**, 233–248 (1983).
59. Z.-D. Zhao, Z. Chen, X. Xiang, M. Hu, H. Xie, X. Jia, F. Cai, Y. Cui, Z. Chen, L. Qian, J. Liu, C. Shang, Y. Yang, X. Ni, W. Sun, J. Hu, P. Cao, H. Li, W. L. Shen, Zona incerta GABAergic neurons integrate prey-related sensory signals and induce an appetitive drive to promote hunting. *Nat. Neurosci.* **22**, 921–932 (2019).
60. K. Nakamura, S. F. Morrison, Central efferent pathways for cold-defensive and febrile shivering. *J. Physiol.* **589**, 3641–3658 (2011).
61. X.-Y. Li, Y. Han, W. Zhang, S.-R. Wang, Y.-C. Wei, S.-S. Li, J.-K. Lin, J.-J. Yan, A.-X. Chen, X. Zhang, Z.-D. Zhao, W. L. Shen, X.-H. Xu, AGRP neurons project to the medial preoptic area and modulate maternal nest-building. *J. Neurosci.* **39**, 456–471 (2019).


**Acknowledgments:** We thank Z. Luo, J. Hu, M. Luo, H. Hu, C. Zhan, P. Cao, and H. Li for reagent share; X. Li and the Molecular Imaging Core Facility (MICF) of School of Life Science and Technology, ShanghaiTech University for microscopic imaging; Y. Xiong and the Molecular Cellular Core for slices and staining; and Z. Gao for data analyzing advice. We also thank all Shen laboratory members and "Shen Xian Hui (NPC)" Wechat group for valuable discussion. We thank the staff members of the Animal Facility at the National Facility for Protein Science in Shanghai (NFPS), Zhangjiang Lab, China for providing technical support and assistance. **Funding:** This study was funded by National Key Research and Development Program of China (2019YFA0801900), Shenzhen-Hong Kong Institute of Brain Science-Shenzhen Fundamental Research Institutions (NYKFKT20190017 to W.L.S.), National Nature Science Foundation of China (31771169 and 91857104 to W.L.S.), and Shanghai Science and Technology Committee of Shanghai City (19140903800). **Author contributions:** W.Z.Y. and X.D. performed most of the experiments. C.G., H.X., Y.X., J.L., and J.X. performed behavioral evaluations. W.Z. performed the electrophysiology. X.J. performed retro-TRAP analysis. X.N., X.Y.F., and H.T. performed the immunostaining. X.F. designed and performed a concurrent recording of BAT and core temperatures. W.Z.Y., J.Y., M.H., H.W., H.Y., X.-h.X., and W.L.S. designed the experiments. W.Z.Y., X.D., and W.L.S. wrote the manuscript. **Competing interests:** The authors declare that they have no competing interests. **Data and materials availability:** All data needed to evaluate the conclusions in the paper are present in the paper and/or the Supplementary Materials and can be obtained from the corresponding author upon reasonable request.

Submitted 31 March 2020
Accepted 17 July 2020
Published 2 September 2020
10.1126/sciadv.abb9414

**Citation:** W. Z. Yang, X. Du, W. Zhang, C. Gao, H. Xie, Y. Xiao, X. Jia, J. Liu, J. Xu, X. Fu, H. Tu, X. Fu, X. Ni, M. He, J. Yang, H. Wang, H. Yang, X.-h. Xu, W. L. Shen, Parabrachial neuron types categorically encode thermoregulation variables during heat defense. *Sci. Adv.* **6**, eabb9414 (2020).